Environ Monit Assess (2023) 195:9
https://doi.org/10.1007/s10661-022-10586-8

Green synthesis, characterization, and application of metal oxide nanoparticles for mercury removal from aqueous solution

Gadissa Tokuma Gindaba ·
Hundessa Dessalegn Demsash ·
Mani Jayakumar

Received: 13 February 2022 / Accepted: 28 June 2022 / Published online: 21 October 2022

Abstract In this work, a novel surface-modified, green-based wheat straw-supported magnetite nanoparticles (Fe_3O_4-NPs) were synthesized via the green synthesis method, and the adsorption of mercury (Hg(II)) ion from aqueous solutions was methodically investigated. The synthesized wheat straw-supported magnetite (Fe_3O_4-WSS) NPs were characterized using X-ray diffraction (XRD), Fourier transform-infrared spectroscopy (FT-IR), thermogravimetric analysis (TGA), and scanning electron microscopic (SEM) methods. FT-IR and TGA confirmed that the surface of Fe_3O_4-NPs was functionalized well. The XRD analysis revealed the existence of magnetite in the synthesized wheat straw-supported Fe_3O_4-NPs of 19.83 nm average crystalline size. SEM analysis showed Fe_3O_4-NPs were almost spherical, with an average particle size of 22.48 nm. Adsorption studies were carried out to investigate the adsorption of Hg(II) ions onto Fe_3O_4-WSS NPs and the effect of various adsorption parameters such as pH, time, adsorbent dosage, and Hg(II) ion concentration. The optimum adsorption conditions were obtained: pH of 6, contact time of 45 min, adsorbate of 40 mg/L, and adsorbent of 1 g. A maximum of 98.04% Hg(II) ion removal efficiency was obtained at these optimum conditions. FT-IR analysis also indicated that surface functional groups such as C = C,–OH, and C–C of the newly produced Fe_3O_4-NPs led to the more efficient removal of Hg(II) from aqueous solution. The synthesized nano-adsorbent showed an excellent adsorption capability of 101.01 mg/g. Hg(II) ions adsorption onto Fe_3O_4-WSS NPs fitted well with the Langmuir adsorption isotherm model. Therefore, these reasonable findings reveal that Fe_3O_4-WSS NPs are an efficient and promising adsorbent for Hg(II) removal from aqueous water environments.

Keywords Adsorption · Biomass · Green synthesis · Mercury removal · Adsorbent · Wastewater

G. T. Gindaba · M. Jayakumar (✉)
Department of Chemical Engineering, Institute of Technology, Haramaya University, P.O. Box 138, Dire Dawa, Ethiopia
e-mail: drjkiothu@gmail.com; drjayakumarmani@haramaya.edu.et

H. D. Demsash (✉)
School of Chemical and Bio-Engineering, Institute of Technology, Addis Ababa University, King George VI Street, P.O. Box 385, Addis Ababa, Ethiopia
e-mail: hundessad@gmail.com; hundessa.dessalegn@aait.edu.et

Introduction

The contamination of water by toxic heavy metals (HMs) has got a great concern owing to their extreme toxicity, non-biodegradability, and carcinogenicity. Heavy metals and, most importantly, emerging pollutants are not well monitored and are causing adverse effects on the environment and public health (Sivaranjanee et al., 2022; Sivasubramaniyan et al.,

2022). The primary sources of emerging contaminants are chemicals, industrial additives, endocrine disruptors, drugs, pharmaceutical compounds, surfactants, and personal care substances that are problematic globally (Khan et al., 2022; Krishnan et al., 2021; Dayana Priyadharshini et al., 2021; Samal et al., 2022). Furthermore, following the enhancement of technological advancement, particularly with further industrialization, emerging pollutants can pollute the water environment and, as a result, causes a great risk to the health of the population (Abbas et al., 2018; Rahman et al., 2022). Ali et al. (2019) studied fossil fuel combustion as one of the causes of heavy metals released into the environment. These HMs contaminate the water, which then leads to severe toxicity and thus endangers the inhabitants of the water environment (Akash et al., 2022). The toxicity of HMs is fatal to living things. The fatality of toxic HMs is caused due to the formation of free radicals that cause oxidative stress, damage to deoxyribonucleic acid (DNA), and main biological molecules like nucleic acids, proteins, lipids, and enzymes (Briffa et al., 2020). Hg(II) is one type of heavy metal mainly used in batteries and switches. Hg(II) is most notably used in thermometers, dental amalgamation, sphygmomanometers, and the amalgamation of silver and gold in mining activities in particular (Nurfatini & Amir, 2018; Rahman et al., 2022). This most toxic heavy metal ion in wastewater or aquatic bodies is mainly released from an oil refinery, battery, chloralkali production, paint manufacturing, paper and pulp, plastic, cement, gold mining, textile, electronic, and rubber processing industries (Altaf et al., 2021; Ghosh et al., 2022).

This highly toxic heavy metal ion causes considerable permanent damage to humans, including hearing loss, vision loss, neurological problems, loss of sensation in extremities, and tremors (Taux et al., 2022). In addition, exposure to Hg(II) generally causes a great risk to the environment, aquatic animals, human health, and economic development (Gallego et al., 2019; Huang et al., 2016). The World Health Organization drinking water quality guideline has set a maximum acceptable concentration edge for Hg in potable water as 0.001 mg/L and placed it on top of the priority list of toxic pollutants (AlOmar et al., 2017). It was also reported that this essential and most toxic heavy metal by the USEPA with a mandatory discharge level of 0.01 mg/L and a maximum acceptable level of 0.001 mg/L of Hg respectively for wastewater and drinking water (Kinuthia et al., 2020). Thus, removing Hg(II) in water is essential and has prodigious prominence.

Different treatment technologies like chemical precipitation, phytoremediation, membrane filtration, ion exchange, adsorption, electrochemical treatment, reverse osmosis, coagulation-flocculation, and biological decomposition have been employed to remove mercury (Al-Zoubi et al., 2015; Rajasulochana & Preethy, 2016). However, most of these techniques are costive, time-consuming, ineffective, and require large quantities of chemicals and high energy to eliminate Hg(II) from the aquatic environment (El-tawil et al., 2019). As an example, chemical precipitation generates unwanted sludge, thus being the cause of secondary pollutants that need further treatment (Camargo et al., 2016). Scholars also reported that membrane technology has high efficiency in separating Hg(II) from water/wastewater; however, the process seems costive due to high energy requirements (Albatrni et al., 2021). Aziz and co-workers reported coagulation/flocculation technique generates large sludge volume and uses non-reusable coagulants and flocculants (Aziz et al., 2018). Similarly, the ion-exchange method is challenging to remove concentrated heavy metal solutions and partially remove specified metal ions (Saleh et al., 2021). However, among the listed methods, employing the adsorption technique, most notably by fabricating functionalized adsorbent, has a superior performance in heavy metal removal. It has the advantages of regenerating adsorbents, high efficiency, low cost, and simple operational processes (Hoang et al., 2022).

Recently, due to rapid advancement in nanotechnology, particularly in nanoscale science and engineering, enormous opportunities have been elevated to advance simple, alternative, flexible, and environmentally tolerable remediation methods. In the case of nanotechnology, nanomaterials are receiving greater attention for the treatment of contaminated water (Arun et al., 2022). They are promising approaches for the effective removal of HMs in water and wastewater by adsorption method due to their easy surface modification, tremendous adsorption capacity, and excellent features resulting from the nanoscale effect (Buzea & Pacheco, 2017; Pandey, 2021). Among the nanometer-sized materials, nanoparticles (NPs) of metal oxide have shown great potential in water treatment, especially for heavy metal exclusion and biomedical uses.

Metal oxide NP adsorbents have several advantages and are in high demand. Easy way of engineering nanomaterials to the required sizes (Jogaiah et al., 2021), easy way preparation techniques, high stability, surface functionalization, high adsorption capacity, relatively high surface area, ability to control their shapes, and reusability are the main advantages of metal oxide NPs or nanomaterials (Naseem & Durrani, 2021; Nikolova & Chavali, 2020). Nano-sized metal oxide NP adsorbents have high selectivity towards the adsorbate. Most commonly, metal oxide NPs such as aluminium oxide, magnesium oxides, nano-sized iron oxides, and zinc oxides have selectivity towards heavy metal pollutants (Naseem & Durrani, 2021). Muldarisnur et al. (2019) showed that the sensitivity of NPs chiefly relies on the morphology of the synthesized nanoparticle adsorbents. The sensitivity of metal oxide NPs is highly dependent on their shape and size than the compositions of NP adsorbents. However, metal oxide NPs adsorbents have disadvantages such as oxidizing with oxygen and water in aqueous solutions (mainly bare metal oxide nanoparticle adsorbents), difficulty in separating from aqueous solutions effectively because of their small size, having aggregation property, having weak affinity to some organic pollutants/or adsorbates (Husein et al., 2021; Yang et al., 2019a, b).

Iron oxide NPs have good advantages in combating environmental contamination from the existing metal oxide NPs. Magnetite NPs (Fe_3O_4-NPs) are gaining significant attention in environmental remediation, moreover, in the removal of HMs owing to their exceptional characteristics viz., great biocompatibility, large surface area to volume ratio, high removal capacity, elevated reactivity, surface modifiability, ease of separation, high selectivity and small particle size which are promising to develop new or improve existing technologies in water/wastewater treatment (Kumar et al., 2021). Nevertheless, Fe_3O_4 NPs made through chemical and physical means result in the loss of reactivity towards the adsorbate, cause the risk of toxicity to the environment, are difficult for reusability, and the protocol uses very reactively and toxic reducing agents (Gebre & Sendeku, 2019). One of the main characteristics of nanoparticles is that the number of atoms found on the surface of nanoparticles is more dominant than the number of internal atoms of nanoparticles, which means the majority of atoms in nanoparticles are located on the surface of nanoparticles (Cuba-Supanta et al., 2022; Wen et al., 2021). The surface atoms that are not saturated can link with extra atoms and hold enhanced chemical activity (Kaur, 2016). The other difficulties with the use of bare Fe_3O_4-NPs include; passivation/oxidation (Zhao et al., 2020), corrosion by non-target compounds, rapid sedimentation that confines the mobility of fine-sized particles in water, and rapid aggregation of the smaller particles that reduce the performance in catching pollutants (Husen & Iqbal, 2019; Marimón-bolívar & González, 2018; Yang et al., 2019a, b). For example, Qiao et al. fabricated superparamagnetic iron oxide NPs and reported that naked Fe_3O_4-NPs spontaneously aggregate and have limited applications (Qiao et al., 2009). Another study also showed bare Fe_3O_4-NPs have poor biodegradability, non-specific interaction, and high chemical instability (Muthiah et al., 2013; Xu et al., 2022).

Thus, to improve the tailbacks innate in the use of Fe_3O_4-NPs for Hg(II) removal, safe and economical way surface modification of Fe_3O_4-NPs still needs extensive research (Khan et al., 2020; Salehipour et al., 2021). The synthesis of Fe_3O_4-NPs by the eco-friendly method is considerably simple and secure, and plant-mediated synthesis of NPs using polyphenol as a reducing agent is still a new scheme. The findings of Singh et al. (2018) and Amin et al. (2021) demonstrated that green synthesis of metal oxide NPs adsorbents is considered a cost-effective, an environmentally friendly, and feasible method for HMs removal.

Green synthesis means the fabrication of nanoparticles using natural sources, benign reagents, nonhazardous solvents, and renewable materials accompanied by processes (Álvarez-Viñas et al., 2022). It generally uses plant parts such as fruits, leaves, flowers, roots, and seeds. Green synthesis of metal oxide nanoparticles is achieved via regulation, remediation, and clean-up production processes (Roohi et al., 2021). Implementing a sustainable and eco-friendly synthesis protocol avoids the fabrication of undesirable and harmful by-products (Malavika et al., 2021). Also, microorganisms counting fungi, bacteria, algae, and viruses can replace toxic chemicals in the synthesis of nanoparticles (Prakash et al., 2022). However, using plant extracts to synthesize metal oxide nanoparticles is the most cost-effective, reproducible, easy process, and the simplest comparative to microorganism

arbitrated synthesis of metal oxide nanoparticles. The availability of phytochemicals in numerous plant extracts, particularly in leaves, such as carboxylic acids, aldehydes, polyphenols, ketones, amides, and terpenoids, enables the synthesis of nanoparticles (Nande et al., 2020). These phytochemicals can reduce metal salts into metal/metal oxide nanoparticles in the synthesis processes.

Therefore, green synthesis of metal oxide nanoparticles and using cheaper, loose, and porous materials as supporting materials can tackle some problems of Fe_3O_4-NPs more (Singh et al., 2019). For example, Govarthanan et al. (2022) studied and successfully synthesized La-MOF@PANI for the effective removal of Pb^{2+} from an aqueous solution and showed adsorption enhancement on the porous surface adsorbent. These materials can be obtained from agricultural waste biomasses. As an agricultural waste, locally available wheat straw requires little processing, and alternative technology can be used as supportive materials (Ebrahimian Pirbazari et al., 2014; Khandanlou et al., 2013). The conformation of wheat straw with Fe_3O_4-NPs can mainly improve the adsorption efficiency and physicochemical properties of Fe_3O_4-NPs. However, the studies on the green synthesis of wheat straw-supported Fe_3O_4-NPs for their application as nano-adsorbent are limited. Thus, using polyphenol-based green synthesized wheat straw-supported Fe_3O_4-NPs improves some of the tailbacks innate in using Fe_3O_4-NPs like stability, reduction in passivation, and corrosion with acids and bases and it also lessens/removes its aggregation.

In this work, functionalized Fe_3O_4-WSS NPs were successfully synthesized by the green synthesis method, systematically characterized, and effectively utilized for Hg(II) ions adsorption from an aqueous solution by batch mode. The adsorption isotherms were carefully explored to remove Hg(II) via the adsorption processes. The adsorption mechanisms during Hg(II) removal were discussed in detail. The impact of different parameters such as solution pH, contact time, initial adsorbate concentration, and adsorbent dosage on adsorption efficiency was investigated. It was found that Fe_3O_4-WSS NPs were a potential nano-adsorbent for the elimination of Hg(II) from aqueous water environments. Thus, this study enables the removal of Hg(II) from aqueous solutions.

Materials and methods

Preparation of wheat straw porous material sample

The wheat straws were collected from the agricultural farm field of Jimma Zone, Gera Woreda, using plastic bags. The collected raw materials were reduced in size (2–6 mm) by cutting into smaller proportions, cleaned several times using distilled water (DH_2O) to exclude dust particles, and dried at 105 °C for 24 h in an oven for the removal of residual moisture content and to acquire the sample with constant mass. Next, the dried wheat straws were ground into fine particles using an electric miller and sieved using a 0.1-mm sieve to avoid unwanted components. The prepared porous material was kept in sealed plastic bags at room temperature until the next stage of the experiments.

Polyphenol preparation from plant extract

Fresh leaves of *Aloe vera* were collected from Jimma zone, Limmu Kosa Woreda. The collected leaves were thoroughly rinsed with DH_2O to exclude foreign and dirt particles and subjected to sun drying for two weeks to remove moisture using the procedure adopted from Burange et al. (2021). The dried leaves were size reduced and made into a powder of 0.1–0.2 mm using an electric miller to prepare the leaf extract. After grinding, 12 g of *Aloe vera* leaf powder was transferred to 100 ml of double- DH_2O and heated in a water bath at 45 °C for 15 min. After vacuum filtration, the resultant extract containing polyphenol was filtered using Whatman filter paper. The filtrate was collected and stored in a refrigerator at 4 °C. The extract was used as an *Aloe vera* extract solution to synthesize magnetite and wheat straw-supported Fe_3O_4-NPs.

Synthesis of magnetite nanoparticles

Fe_3O_4-NPs were prepared by the reduction of $FeCl_2.4H_2O$ (99%) and $FeCl_3.6H_2O$ (99%) (Finkem, Italy) solution in the presence of *Aloe vera* polyphenol extract. $FeCl_2.4H_2O$ and $FeCl_3.6H_2O$ were taken in 1:2 w/w ratios (Yang, 2012) and then dispensed in 200 mL of deionized water into a 500 mL beaker.

Next, 12 mL of Aloe vera polyphenol extract was added to this solution under mild string with a magnetic stirrer. A solution of 2 M of NaOH (99.8%) (ATDM, Turkey) was prepared and added drop-by-drop until the solution's pH reached 11.5 and then stirred continuously until the solution was changed to black, showing the formation of precipitates. The solution was left undisturbed, and the black-colored precipitates were deposited at the bottom of the flask. The precipitates were isolated after decanting the solution and washed twice with deionized water. After a whole, the solution was subjected to centrifugation at 5000 rpm for 20 min. The centrifugation and washing processes were repeated three times. Then, the precipitates were carefully collected into an oven-dried Petri dish and oven-dried at 60 °C for 12 h. Finally, the synthesized solid NPs (Fe_3O_4) were kept appropriately for characterization purposes.

Synthesis of wheat straw-supported magnetite nanoparticles

Wheat straw-supported Fe_3O_4-NPs were prepared by the reduction of $FeCl_2.4H_2O$ (99%) and $FeCl_3.6H_2O$ (99%) solution in the presence of *Aloe vera* polyphenol extract. $FeCl_2.4H_2O$ and $FeCl_3.6H_2O$ were taken in 1:2 w/w ratios and then dissolved in 200 mL deionized water into a 500-mL beaker. After the solution was prepared, 3 g of ground wheat straw and 12 mL of *Aloe vera* polyphenol extract were transferred to the solution and heated at 80 °C under mild string with a magnetic stirrer (magnetic stirrer containing a hot plate). A solution of 2 M of NaOH (99.8%) (ATDM, Turkey) was prepared and added drop-by-drop until the solution's pH reached 11.5 and then stirred continuously until the solution was changed to black, showing the formation of wheat straw-supported Fe_3O_4-NPs. The formed black-colored precipitates were deposited at the bottom side of the flask and kept undisturbed for separation purposes. The precipitates were isolated after decanting the solution, followed by washing with deionized water twice. After a whole, the solution was subjected to centrifugation at 5000 rpm for 20 min considering the protocol adopted (Lazzarini et al., 2021). The centrifugation and washing processes were repeated three times. Then, the precipitates were carefully collected into an oven-dried Petri dish and oven-dried at 60 °C for 12 h. Finally, the synthesized adsorbent was named wheat straw-supported magnetite (Fe_3O_4-WSS) NPs and kept in an appropriate place for characterization and adsorption studies.

Characterization of synthesized Fe_3O_4-WSS nanoparticles

The synthesis of Fe_3O_4 NPs was confirmed by UV–visible spectral analysis. A small aliquot of the supernatant of the synthesized Fe_3O_4 or Fe_3O_4-WSS NPs was used for analysis purposes. Accordingly, the characteristic absorption peak for the synthesized Fe_3O_4-NPs was analyzed using UV–visible absorption spectroscopy in the wavelength range of 300 to 700 nm. The crystallite size and crystallinity of green synthesized Fe_3O_4-WSS NPs were examined with XRD (X-ray diffraction, DW-XRD-Y7000) analysis. For this, well dried and powdered samples were used. It was operated at 30 kV and 25 mA with CuKα radiation ($\lambda = 0.154021$ nm). The scanning was done from 10 to 80° with steps of $0.03°s^{-1}$ to collect 2θ data. Phase and pattern analysis of the XRD data was studied using Match! Software version 3.10.2.173 and Origin Pro2019b version 9.65. Most characterization techniques were adopted (Alfredo et al., 2020; Sandhya & Kalaiselvam, 2020). The average crystalline size of Fe_3O_4-WSS NPs was calculated using Scherrer's Eq. (1).

The surface functionalization of the synthesized Fe_3O_4-WSS NPs was determined with the help of FT-IR spectroscopy (Fourier transform infrared-spectroscopy, Perkins Elmer L1600300). The synthesized adsorbent was dried, ground, and mixed with KBr powder in appropriate ratios to make a pellet for FT-IR spectroscopy analysis before and after the adsorption experiments. These measurements were executed, and the spectra were collected in the range of 4000–400 cm^{-1}. The structure and morphology of synthesized Fe_3O_4-WSS NPs were examined by Scanning Electron Microscope (SEM) (JCM-6000Plus). The acceleration voltage for the SEM was set at 15 kV. Origin Pro 2019b version 9.65 and ImageJ version 1.44 software were used to analyze the synthesized Fe_3O_4-WSS NPs further using the results of SEM analysis. Thermogravimetric (TG) analysis of Fe_3O_4-WSS NPs was executed for powder samples (~8 mg) with a heating rate of 10 °C/min from 25 up to 800 °C using Perkin-Elmer TGA-4000 TG in a nitrogen gas atmosphere. Origin Pro 2019b version

9.65 was used to execute and analyze the Derivative TG Data (DTD).

$$D = \frac{\kappa\lambda}{\beta\cos\theta} \quad (1)$$

where D = mean crystalline size; κ = Scherrer's constant (shape factor) with the − value of 0.9; λ = X-ray wavelength (0.154021 nm); β = full width at half maximum (FWHM) in radians; θ = Bragg angle.

Adsorption experiments

A stock solution of 1 g/L Hg(II) was prepared by dissolving a 1.354 g analytical grade of $HgCl_2$ (99%) (Finkem, Italy) in 1L DH_2O. As experimental solutions, a series of diluted Hg(II) solutions (20, 40, 60, 80, and 100 mg/L) were used. Various batch experiments were done by wheat straw supported Fe_3O_4 NPs using different dosages of MNP-WSS (0.1, 0.4, 0.7, 1, and 1.3 g), initial pH of (2, 4, 6, 8, and 10), initial contact times of (15, 35, 55, 75, and 95 min), and initial Hg(II) concentrations of (20, 40, 60, 80, and 100 mg/L). All adsorption experiments were carried out at 25 ± 2 °C temperature, and 0.1 M NaOH and 0.1 M HCl (36.46%) (LOBA Chemie, India) were used for the correction of pH. In each experiment, a specified dosage of MNP-WSS was added to the noted concentration of Hg(II) solution in a 250 mL conical flask. The solution volume of each experiment was 100 mL. The mixture was mixed by a mixer for different contact times at 250 rpm. After given contact time, each sample was centrifuged for 5–10 min, filtered by a membrane filter, and analyzed for Hg(II) residuals. The absorbance of Hg(II) residuals was analyzed by UV–Visible spectrophotometer at a wavelength of 490 nm, and the Hg(II) residues concentration was analyzed based on the calibration curve. All the adsorption experiments were performed with three replicates, and the average of obtained values was considered for further analysis. The removal efficiency (R) of Hg(II) was calculated by Eq. (2).

$$R(\%) = \frac{C_o - C_e}{C_o} \times 100 \quad (2)$$

where C_o and C_e are initial and equilibrium liquid phase solute concentrations in mg/L, respectively.

The mass of Hg(II) adsorbed/g of Fe_3O_4-WSS NPs adsorbent was calculated as below:

$$q_e = \frac{C_o - C_e}{M} \times V \quad (3)$$

where q_e is the amount of Hg(II) that was adsorbed, C_o is the Hg(II) concentration of the solution before the equilibrium (mg/L), C_e is the Hg(II) concentration of the solution in the equilibrium (mg/L), M is the mass of adsorbent (MNP-WSS) (g), and V is the volume of Hg(II) solution (sample solution) (L).

UV–visible spectrophotometer analysis of mercury(II) concentration

The residual concentration of Hg(II) was analyzed by preparing a calibration curve as reported by (Elly & Elly, 2014; Vega-Páez et al., 2019). A total of 1 g/L stock solution of Hg(II) was prepared by dissolving 1.354 g analytical grade of $HgCl_2$ (99%) in 1 L DH_2O containing 2 mL of HNO_3 (69.5%) (LOBA Chemie, India) in a volumetric flask and a series of diluted Hg(II) solutions (10, 20, 40, 60, 80 and 100 mg/L) were prepared from a stock solution. A solution of 1, 5-diphenylcarbazide (98%) (Merck, Germany) was prepared by dissolving 0.4 g of diphenylcarbazide in 100 mL of methanol (99.9%) (Merck, Germany) in a 150-mL volumetric flask. In total, 1–1.5 mL of a prepared solution of diphenylcarbazide was added to each diluted Hg(II) to develop a colorful solution, and the pH of Hg(II)—diphenylcarbazide mixture was adjusted to a pH of 5–6 (for calibration curve only) using 0.1 M of NaOH (99.8%) and HCl (36.46%) to avoid background interference during UV–visible spectrophotometer analysis. After the whole, the absorbance of a known concentration of each diluted Hg(II) was performed by a UV–visible spectrophotometer at a wavelength of 490 nm. 1 ml of a prepared solution of diphenylcarbazide was used for the UV–visible spectrophotometric analysis through each experimental batch.

Langmuir and Freundlich isotherms

The Langmuir and Freundlich adsorption isotherm models are stated as Eqs. (4) and (6).

$$\frac{C_e}{q_e} = \frac{1}{bq_{\max}} + \frac{C_e}{q_{\max}} \quad (4)$$

In another way, using constant b, equilibrium limit (R_L) can be computed by Eq. (5).

$$R_L = \frac{1}{1 + bC_o} \quad (5)$$

$$\frac{X}{M} = KC_e^{1/n} \quad (6)$$

where q_e (mg/g) is the adsorbed adsorbate; C_e (mg/L) is the concentration at equilibrium; $q_{\max}$ (mg/g) is the monolayer capacity; b (L/mg) is constant for Langmuir: Where K and n are measurements for Freundlich.

Determination of point of zero charge

A salt solution of 0.010 M NaCl (99.5%) was prepared in a conical flask to determine the point of zero charges. 0.10 g of MNP-WSS and 50 mL of 0.010 M NaCl solution were mixed in nine separate conical flasks at ambient temperature (25 °C) and well tight. The pH of the mixtures was corrected to an initial pH value of 2, 3, 4, 5, 6, 7, 8, 9, and 10 by adding many drops of 0.01 M HCl or NaOH solution and was agitated manually. The agitated mixtures were maintained for three days, and the final pH was carefully determined with a digital pH meter. The plot of the difference in final pH and initial pH versus initial pH was constructed, and the pH of point of zero charges (pH_{pzc}) was obtained as the intercept on an x-axis of the plot.

Results and discussions

Characterization of synthesized Fe_3O_4-WSS NPs

UV–Visible spectrophotometer analysis

The UV–Visible spectrum of the formed Fe_3O_4 NPs is depicted in Fig. 1a. The typical surface plasmon resonance absorption peak at 380 nm by UV–Visible spectroscopy revealed the formation of Fe_3O_4 NPs. This confirms the synthesis of Fe_3O_4 NPs by reducing ferrous chloride tetrahydrate and ferric chloride hexahydrate solution using *Aloe vera* leaf extract containing polyphenol as a reducing and capping agent (López & Antuch, 2020). Furthermore, a corresponding study of UV- Vis spectra of *Aloe vera* leaf extract has been shown to confirm the formation of Fe_3O_4NPs, as the iron oxide NPs have been reported to possess absorption bands between 330 and 450 nm (Vélez et al., 2016).

Fourier transform infrared spectrum analysis

Functional groups and surface functionalization were distinguished by Fourier transform infrared (FT-IR) spectroscopy. The result from the FT-IR spectrum showed that there were different functional groups present on the surface of the synthesized Fe_3O_4-WSS NPs (Fig. 1b). Figure 1b shows the FT-IR spectra of *Aloe vera* leaf powder extract (black) and wheat straw powder (red). The broad spectrum peaks in the band of 3650–3200 cm^{-1} were assigned to the –OH functional groups from phenol and cellulose of *Aloe vera* extract and wheat straw powder. The bands at 1646 cm^{-1} and 1640 cm^{-1} match with that of the alkene C=C stretching vibrations functional group. Also, the band in the 1250–1010 cm^{-1} almost represents the vibration of the C–O functional group in phenols, lignin, cellulose, alcohols, carboxylic acids, and ethers. The absorption peak observed at 2923 cm^{-1} and 2906 cm^{-1} is because of the presence of the C–H stretching of alkanes. In the same way, the band at 610 cm^{-1} and 612 cm^{-1} demonstrates the C–Cl bond of alkyl halides. The formation of these hydroxyl and carbon groups may be due to *Aloe vera*, a biomass precursor containing carbon and oxygen-rich complexes (Malavika et al., 2021). The current study's findings are consistent with the previous study of Azizi Haghighat and Ameri (2016), which revealed that Fe_3O_4 NPs could be surface functionalized and modified using biomass. Similarly, Kavitha et al. (2022) studied the production of CuO·NPs using *Abrus precatorius* leaf extract and showed the possibility of producing surface-functionalized nanoparticles using plant extracts.

Figure 2(a) presents the FT-IR spectrum of biosynthesized Fe_3O_4-WSS NPs. As can be seen from Fig. 2(a), the broad peak at 3456 cm^{-1} in the band of 3640–3200 cm^{-1} represents OH stretching vibrations of phenol and/or cellulose, the sharp peak at 1636 cm^{-1} corresponds to the C=C stretching, and the peak at 581 cm^{-1} in the spectrum was allotted

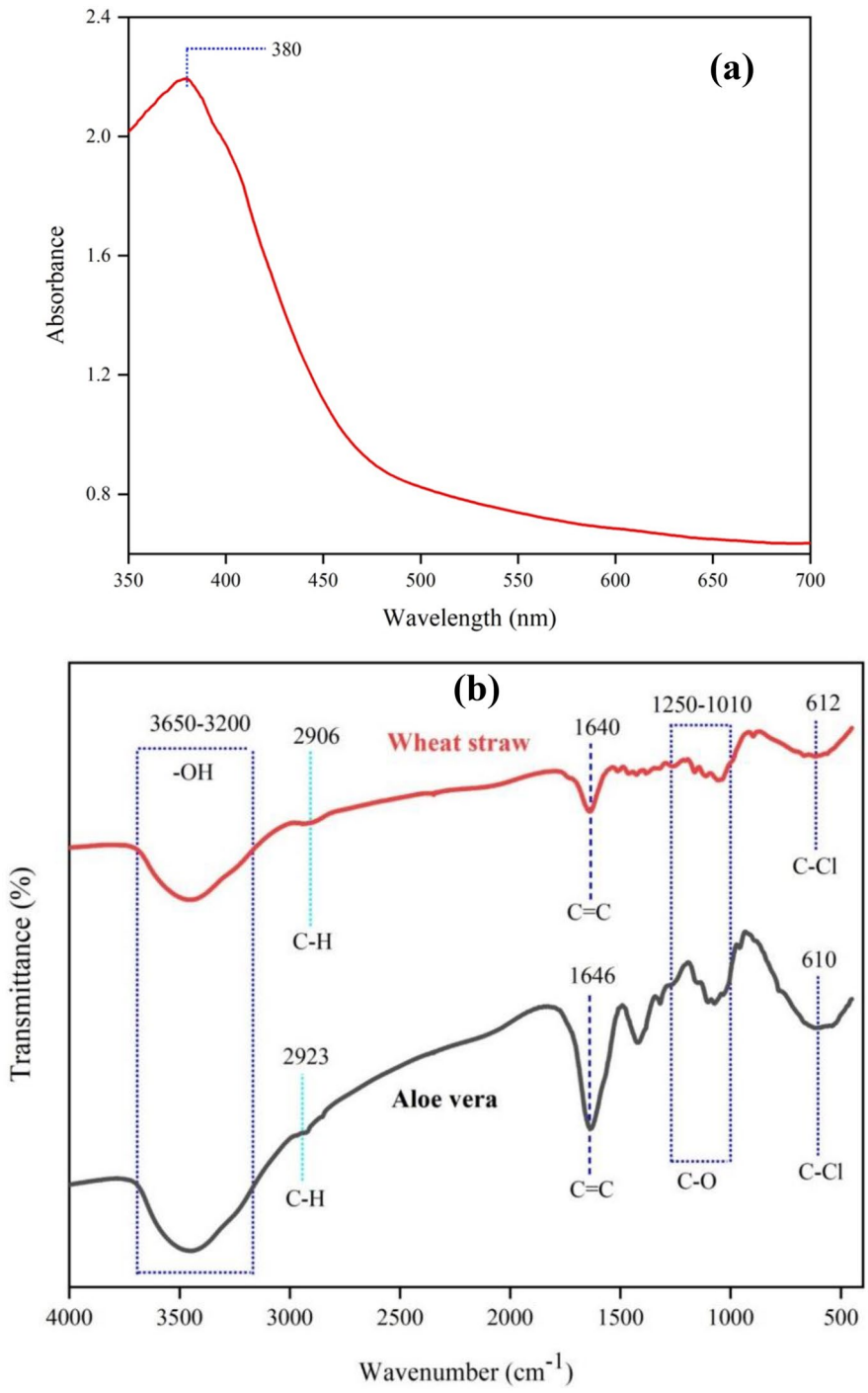

Fig. 1 **a** UV – visible absorption spectra of the synthesized Fe_3O_4-WSS NPs; **b** FTIR spectra of wheat straw (red) and *Aloe vera* extract (black).

to the Fe–O bond on the surface of the synthesized Fe_3O_4-WSS NPs. The absorbance of the peaks at 2893 cm^{-1} and in the band 1250–1010 cm^{-1} revealed the C–H stretching vibrations and C–O functional groups, respectively. Thus, the result from the FT-IR spectrum indicates the functionalization of magnetite NPs by different functional groups and the effective binding of WS on the surface of Fe_3O_4 NPs.

Phenol has exceptional chemical power to reduce NPs and at the same time to successfully

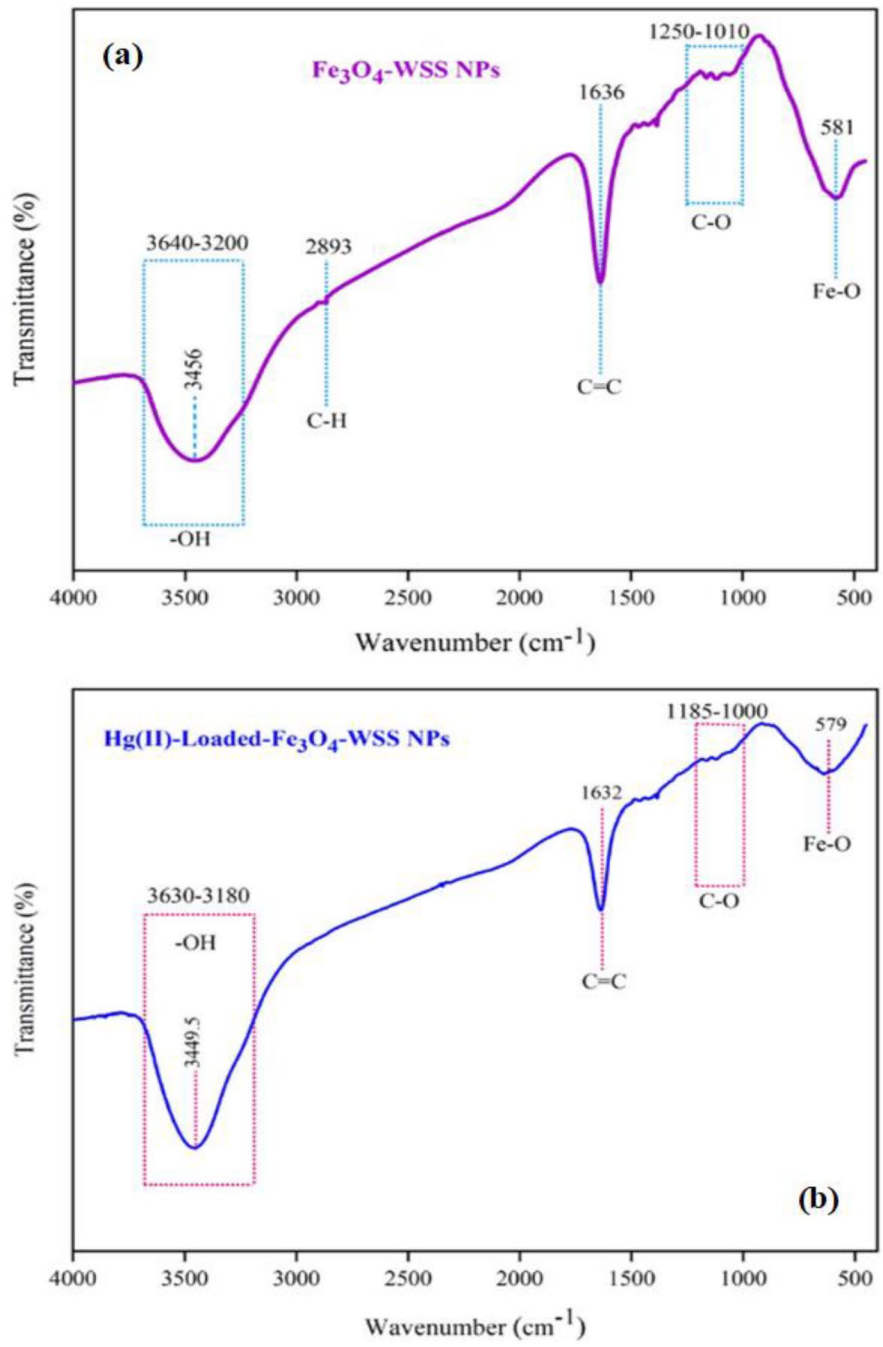

Fig. 2 FT-IR spectra of synthesized Fe_3O_4-WSS NPs before Hg (II) adsorption **a** and after Hg(II) adsorption **b**

cape NPs, therefore enhancing their stabilization. This is owing to the existence of hydroxyl functional groups of a phenolic compound that can bind to metals in the synthesis of NPs (Rauwel et al., 2015). Moreover, the existence of the above listed functional groups on the surface of the synthesized Fe_3O_4-WSS NPs showed that the *Aloe vera* extracts and WS served in stabilizing and, therefore, inhibiting/reducing the NPs from adhering and agglomeration, which makes NPs effective for HMs removal (Azizi Haghighat & Ameri, 2016). The FT-IR spectra of Fe_3O_4-WSS NPs before and after Hg(II) adsorption are shown in Fig. 2(a) and (b), respectively. The analyses were executed to establish the

adsorption mechanism of Fe_3O_4-WSS NPs adsorbent before and after Hg(II) adsorption.

Comparing the FT-IR spectra of Fe_3O_4-WSS NPs and Hg(II) loaded Fe_3O_4-WSS NPs, Fig. 2(b) shows the shift of peaks from 3456, 1636, and 581 cm^{-1} before adsorption of Hg(II) to 3449.5, 1632, and 579 cm^{-1} after adsorption of Hg(II) indicates the stretching vibration of –OH, the stretching vibration of C=C and the Fe–O stretching vibration of these represented functional groups respectively. These slight peak shifts are observed due to the involvement of these major functional groups in the adsorption of Hg(II) ions. The shift in a peak at 3449.5 cm^{-1} for hydroxyl groups has occurred most likely due to the participation of –OH groups in Hg(II) adsorption. The change and the decrease in the stretching vibration of the Fe–O bond after adsorption, which was represented at 579 cm^{-1}, showed the synergy of Fe–O with Hg(II); thus, it confirms that Fe–O played a significant role in Hg(II) adsorption. In another way, the shift of the band from 1636 to 1632 cm^{-1} after adsorption portrays the successful linking of Hg(II) ions to the active sites of alkenes (C=C). This happened because alkenes (C=C) have major active sites for binding metals/ HMs (Vs et al., 2017).

Similarly, the shift of the bands from 1250–1010 cm^{-1} to 1185–1000 cm^{-1} disclosed the participation of C–O functional groups in the adsorption of Hg(II) ions. This was because C–O functional groups have effective active sites that can be involved in binding HMs by ion exchange and/or ionic interactions. As reported by previous studies, these functional groups have effective potential to remove HMs (Ebrahimian Pirbazari et al., 2014; Krishnani et al., 2021).

X-ray diffraction analysis

Figure 3 illustrates the X-ray powder diffractograms of the wheat straw supported (Fe_3O_4-WSS NPs) (top) and the unsupported (bottom).

The characteristic peaks at 2 θ values of 30.52, 35.64, 43.3, 53.38, 57.48, and 62.87, indexed to their Miller indices of X-ray diffraction (XRD) peaks 220, 311, 400, 422, 511, and 440, respectively, demonstrating the existence of magnetite in the synthesized Fe_3O_4-WSS NPs. These peaks were stable with that of the standard XRD data for the cubic structure of Fe_3O_4 NPs JCPDS file (PCPDFWIN v.2.02, PDF No. 85–1436). The wheat straw-supported Fe_3O_4 NPs

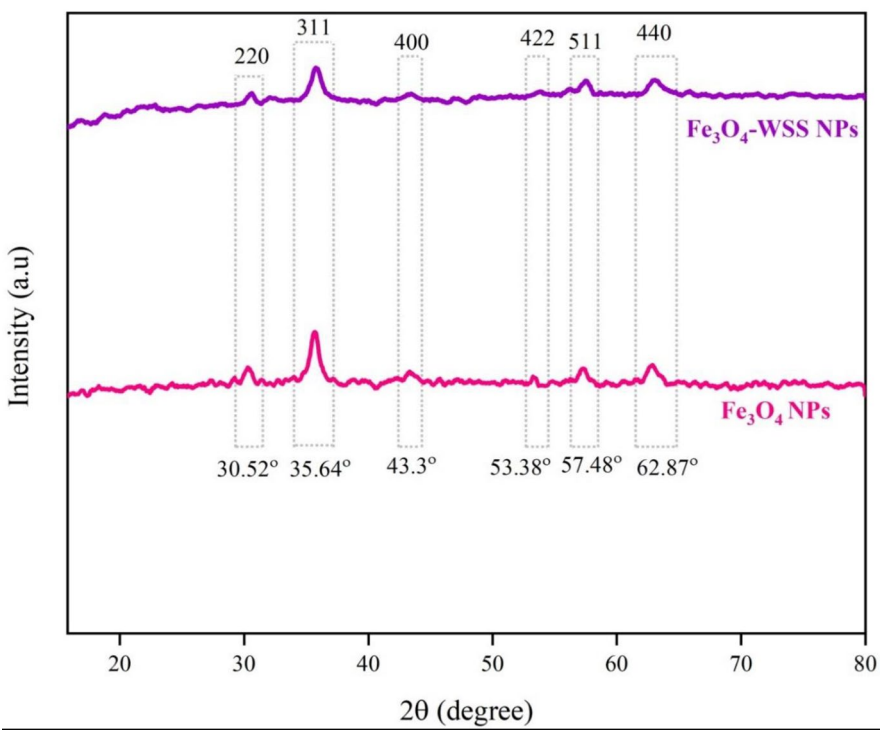

Fig. 3 XRD patterns of the wheat straw supported (top) and the unsupported (bottom) Fe_3O_4 NPs

showed similar peaks as the unsupported Fe_3O_4-WSS NPs, indicating that the WS interaction had no impact on the phase change and it did not degrade the core of Fe_3O_4 NPs. Nonetheless, as shown in Fig. 3, in the case of wheat straw-supported Fe_3O_4 NPs, the height of the peaks decreased, and the background became almost noisier, which shows the peak reflections are generated from the core Fe_3O_4 NPs. It has also been distinguished that the increase in the width of the peaks indicates the reduced crystalline size and the low crystallinity of Fe_3O_4 NPs (Silva et al., 2013). The average crystalline size of the synthesized Fe_3O_4-WSS NPs was calculated from the FWHM (Table 1) of the reflection planes of the XRD data using Debye–Scherrer's formula (1) and was found with an average crystalline size of 19.83 nm.

Scanning electron microscope analysis

Figure 4(a) and (b) illustrate the scanning electron microscopy image of unsupported Fe_3O_4 (a) and WS-supported Fe_3O_4 (b) NPs separately. The images show that the WS-supported Fe_3O_4 NPs are predominantly nearly spherical and rod-like shapes. After surface-modified, the adsorbents/NPs dispersion was enhanced, and the aggregation was reduced. The reduction in the aggregation of Fe_3O_4-WSS NPs is most probably supporting wheat straw weakens the magnetic interactions amongst NPs. As shown in Fig. 4(a), the non-supported Fe_3O_4 NPs were bunched and were not dispersed well. Instead, they were more agglomerated by forming mud-like dried structures. This was most probably due to the effect of magnetic properties of the synthesized Fe_3O_4 NPs increasing nanoparticle interactions (Somu et al., 2019).

Aggregation decreases the reactive surface area of NPs, which results in decreasing the adsorption efficiency of NPs. In another way, the average particle size of the synthesized Fe_3O_4-WSS NPs was analyzed from the result of the (scanning electron microscope) SEM image (Fig. 4(b)) using (ImageJ software and Origin Pro 2019b) and was found to be 22.48 nm as illustrated with histogram Fig. 4(c) with a polydispersity of 0.37(37%). The calculated polydispersity value was very far from one (100%), and at the same time, the average crystalline size and average particle size were almost nearer to each other, confirming that the synthesized Fe_3O_4-WSS NPs were predominantly monodispersed (Mahbubul, 2019). Monodispersed NPs have the lowest agglomeration property. Thus, the analyzed property indicates that the agglomeration of the synthesized Fe_3O_4-WSS NPs was lessened. The average particle size of Fe_3O_4-WSS NPs was compared with the work of different researchers (Table 2) and was found to have a relevant average particle size.

Thermogravimetric analysis of the synthesized adsorbent

TGA was performed to identify the decomposition temperature and thermal stability of Fe_3O_4-WSS NPs and most probably to determine the approximate extent of surface modification of Fe_3O_4, as depicted in Fig. 5. The 6.14% weight loss at the start of the (thermogravimetric analysis) TGA curve (below 180 °C) was due to the evaporation and dehydration of adsorbed and surface water from the synthesized Fe_3O_4-WSS NPs (endothermic process). The second (II) and third (III) regions from 203 to 305 °C and from 306 to 502 °C, which accounts for the total loss of 30.38%, could be due to the thermal decomposition/combustion of capping agents and/or the decomposition of organic groups from the surface of Fe_3O_4-WSS NPs. After

Table 1 Parameters derived from XRD data analysis of the synthesized Fe_3O_4-WSS NPs (Match! software analysis result and calculated values)

$d(A_o)$	$d(A_o)$ calculated	2theta	*h*	*k*	*l*	FWHM	Crystalline size (nm)	Av. crystalline size (nm)
2.929	2.927	30.52	2	2	0	0.374	22.018	19.83
2.519	2.517	35.64	3	1	1	0.540	15.447	
2.090	2.088	43.3	4	0	0	0.371	23.038	
1.716	1.715	53.38	4	2	2	0.362	24.563	
1.603	1.602	57.48	5	1	1	0.480	18.876	
1.478	1.477	62.87	4	4	0	0.620	15.015	

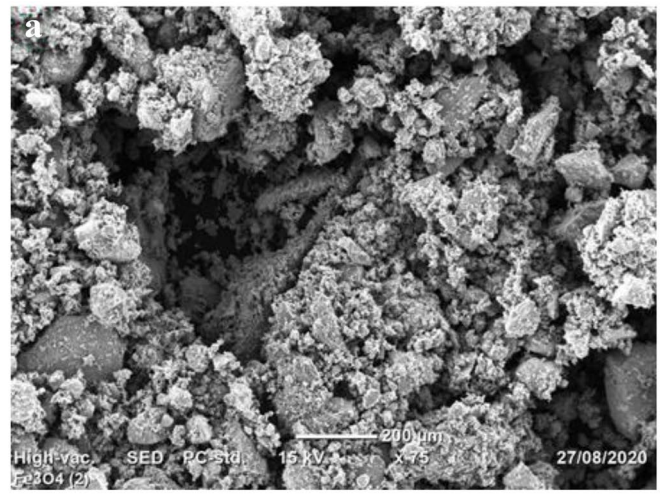

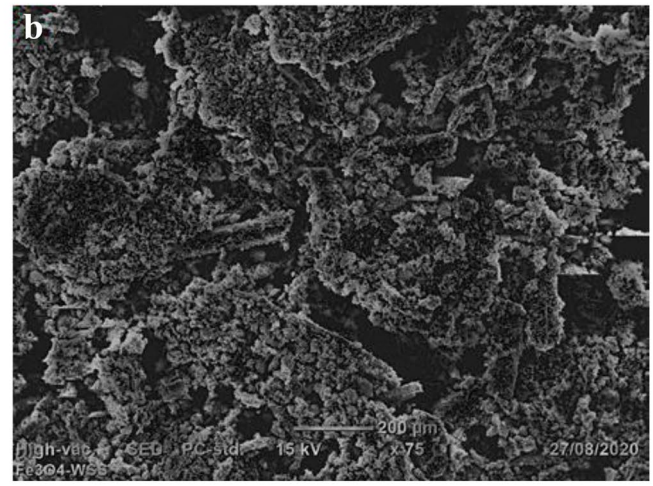

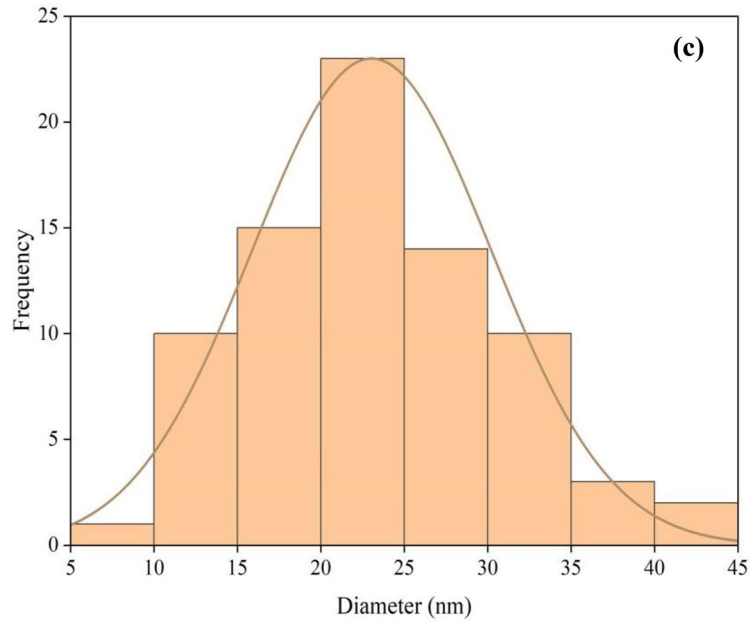

Fig. 4 **a** SEM images of the synthesized Fe_3O_4 NPs; **b** SEM images of the synthesized Fe_3O_4-WSS NPs; **c** Particle size distribution histogram representation of the SEM image of the synthesized Fe_3O_4-WSS NPs.

Table 2 Comparison of average particle size of Fe_3O_4-WSS NPs with related adsorbents

Adsorbent type	Average particle size (nm)	References
DHPCT@Fe_3O_4 MNPs	17	Venkateswarlu and Yoon (2015)
Fe_3O_4-SiO_2	20	Yazdani et al. (2016)
Functionalized Fe_3O_4	17	Scopel et al. (2019)
CCMN	30	Rahbar et al. (2014)
IONP-ASC	28.1	Gruskiene et al. (2018)
Fe_3O_4-WSS	22.48	This study

the third stage, the TGA curve remained almost constant, and there was no weight loss observed from the curve, which shows Fe_3O_4 was only present and was stable above 502 °C. The result from TGA/DTG indicates that different functional groups exist on the surface of Fe_3O_4-WSS NPs. Pakzad et al. (2019) also reported similar findings for biosynthesized Fe_3O_4 NPs that revealed the decomposition occurs due to the capping agent and/or existing organic components.

Determination of point of zero charge

The point of zero charges of an adsorbent is a significant characteristic parameter that determines the net surface charge of the ion in a given solution. It specifies the electrical neutrality of the adsorbent at a specific pH; thus, the charge on the surface of a specific adsorbent becomes zero. Figure 6 indicates the result of the pH of point of zero charges (pH_{pzc}) of Fe_3O_4-WSS NPs determined by a salt solution method. Accordingly, the pH_{pzc} of Fe_3O_4-WSS nanoadsorbent was measured to comprehend the change of surface character of the synthesized adsorbent under varying pH values and was determined to be 4.32 (Fig. 6). This shows that the surface of Fe_3O_4-WSS NPs is positively charged at solution $pH < pH_{pzc}$ (4.32), however, at solution $pH > pH_{pzc}$ (4.32), the surface of Fe_3O_4-WSS becomes negatively charged. Therefore, there is high Hg(II) adsorption when the pH of the solution is above pH_{pzc}. Since the surface of Fe_3O_4-WSS NP adsorbent is positively charged at

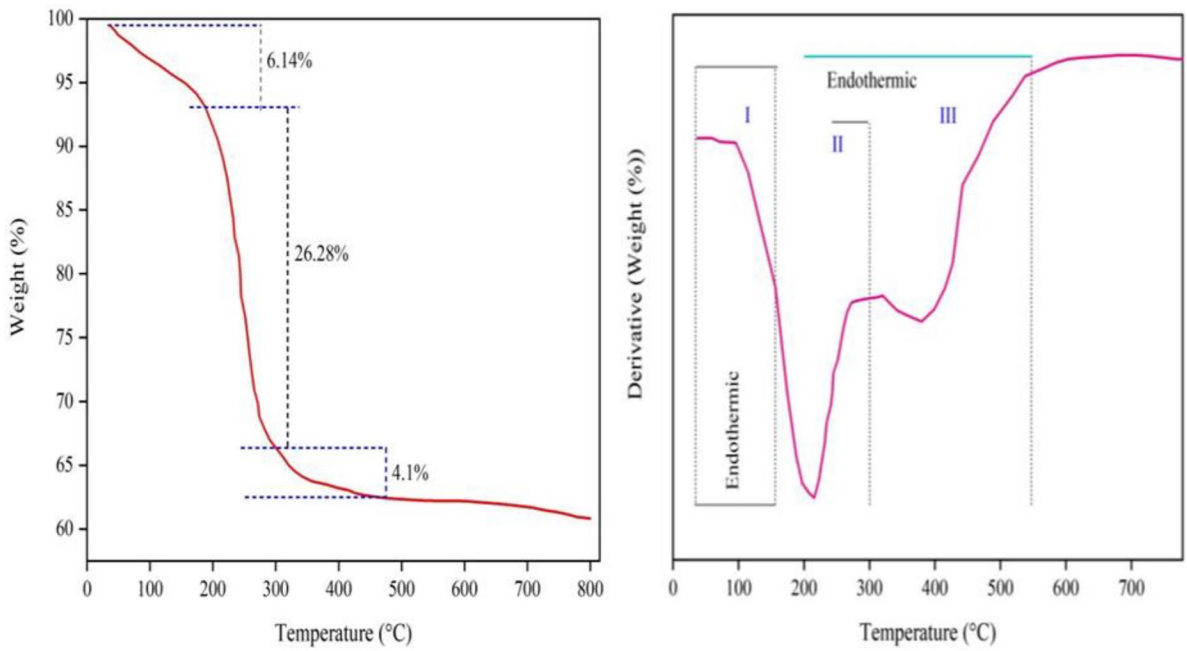

Fig. 5 TGA and DTG curves of Fe_3O_4-WSS NPs

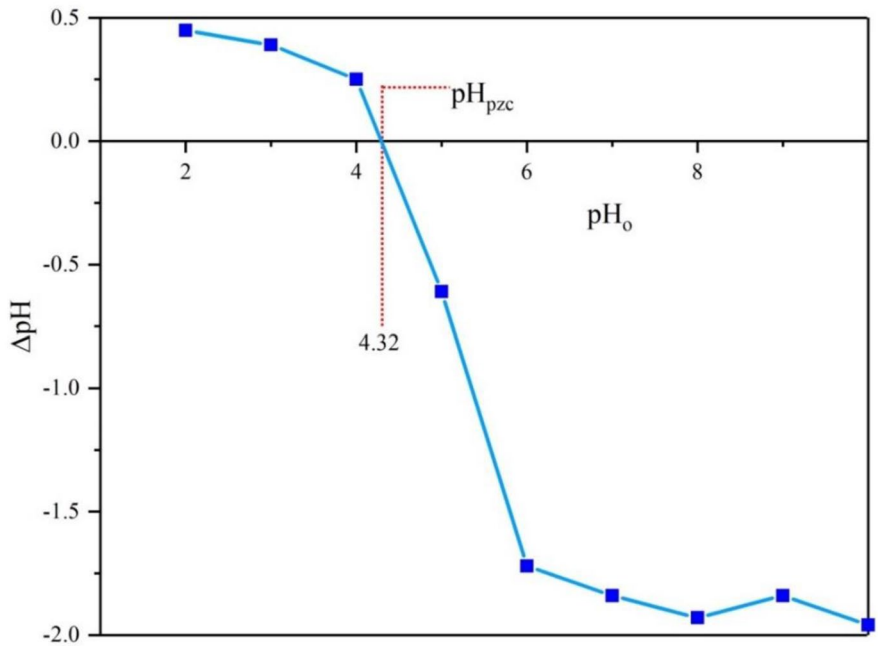

Fig. 6 Point of zero charge

pH < 4.32; thus, they can adsorb anions from an aqueous solution.

Mercury (II) removal studies

Effect of the pH solution on Hg(II) removal

The impact of the pH on Hg(II) elimination was assessed at room temperature using a 100 mL of 40 mg/L initial Hg(II) solution in the pH range of 2–12, with an adsorbent dose of 0.7 g, shaking speed of 250 rpm and a contact time of 75 min. As shown in Fig. 7(a), Hg(II) adsorption on Fe_3O_4-WSS NPs mainly depends on solution pH, and the minimum and maximum adsorption efficiency appeared at pH 2 and 6, respectively. It was known that in the aqueous solution, mercury species mainly exist at different pH values as $Hg(OH)^+$, $Hg(OH)_2$, and Hg^{2+} (Abbas et al., 2018). These species have a significant effect on the adsorption processes. At low pH, the electrostatic repulsion between the positive charges of Fe_3O_4-WSS nano-adsorbent and the cationic species of Hg(II) results in poor removal efficiency of Hg(II). There is a competition of hydrogen ions with cationic Hg(II) species for binding sites on Fe_3O_4-WSS NPs. This happened because; the excessive presence of H^+ occupied the active surface sites of Fe_3O_4-WSS NPs, ensuing in the competition adsorption among Hg(II) and H^+, resulting in the decline of Hg(II) adsorption.

Moreover, at $pH < pH_{pzc}$, increasingly positively charged adsorbent surface and more positively charged metal ions are attributed to electrostatic repulsion, prohibiting interaction between the adsorbent and metal ion (Xiang et al., 2021). As the solution pH increased, more electronegative charges were made on the surface of the nano-adsorbents; therefore, there is an electrostatic attraction between the cationic species of Hg(II) and the adsorbent, and accordingly, the adsorption capacity of Fe_3O_4-WSS NPs sustained to increase. However, as depicted in Fig. 7(a), at higher solution pH, the removal of Hg(II) ions decreased, which may be happened because of the formation of Hg^{2+} ions as hydroxide complexes.

In another way, in an aqueous solution, the surface of Fe_3O_4-WSS NPs acquire a surface charge in the deprotonation or protonation of the FeOH surface site, which can play a vital role in the metal ion removal (Ahmed et al., 2013). The process of protonation or deprotonation of the FeOH surface site depends on the pH_{pzc} of the Fe_3O_4-WSS nano-adsorbent and the solution pH. At $pH < pH_{pzc}$, protonation occurs, thus, Fe-$(OH_2)_n^+$ are the leading type for Fe_3O_4-WSS NPs, and as a result, the protonated adsorption sites make the Hg(II)

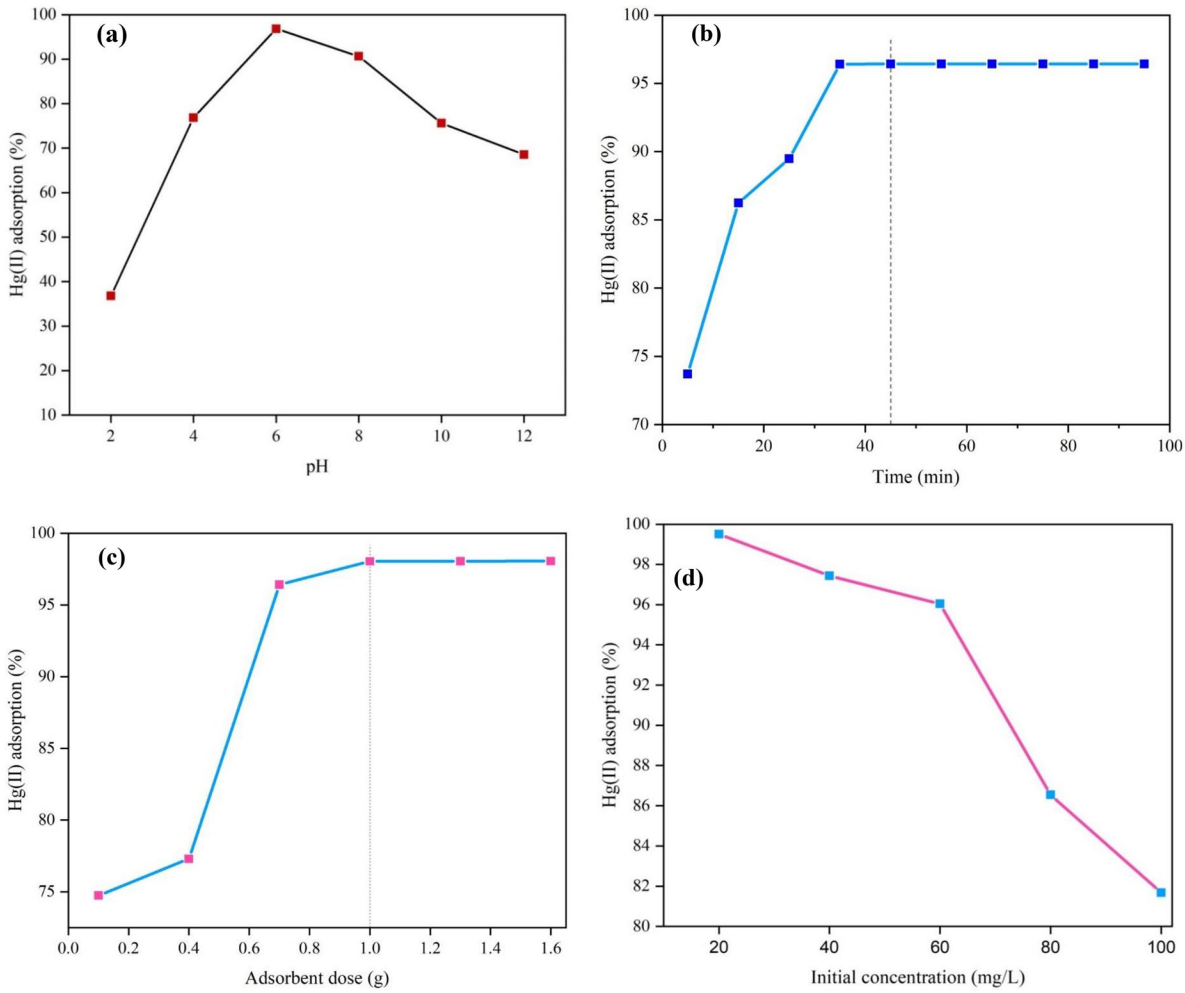

Fig. 7 **a** Effect of the pH on the removal of Hg (II); **b** Effect of the contact time on Hg (II) removal; **c** Effect of adsorbent dosage on Hg (II) removal; **d** Effect of initial concentration on Hg(II) removal.

adsorption unfavorable owing to electrostatic repulsion between positively charged sites and positively charged metal ions. However, at $pH > pH_{pzc}$, $Fe–O^- + H^+/Fe–O–(OH)_n$ are predominant, and therefore the deprotonated adsorption sites make the Hg(II) adsorption favorable because of electrostatic attraction for Hg(II) on to the negatively charged sites. These findings well corroborate with the previous findings of Guo et al. (2016) and He et al. (2021), showing that the pH of the solution has a serious effect on the Hg(II) degradation process because it determines both the speciation of Hg(II) in the solution and the surface charge of the synthesized nanoadsorbent. Then the optimum pH solution for Hg(II) ions adsorption by Fe_3O_4-WSS NPs was chosen as pH 6.

Effect of the contact time on Hg(II) removal

The contact time effect on Hg(II) removal was conducted at room temperature from 5 to 95 min with 10 min time intervals and using a 100 mL of 40 mg/L initial Hg(II) solution with an adsorbent dose of 0.7 g, shaking speed of 250 rpm and pH of 6.

The experimental result for the effect of contact time is shown in Fig. 7 (b). According to Fig. 7 (b), the adsorption rate of Hg(II) ions onto the adsorbent Fe_3O_4-WSS NPs increased rapidly with increasing

contact time (5–25 min). It was found that about 73.71% of Hg(II) ions were removed throughout the initial 5 min showing the adsorption of Hg(II) ions onto Fe_3O_4-WSS NPs was very fast at the first stage of the adsorption processes. This is due to the existence of a large number of free negatively charged active binding sites (Awual, 2017), such as (OH, C=C, C–O) on the surface of the adsorbent Fe_3O_4-WSS NPs, thus resulting in the rapid removal of Hg(II). The effective binding of the surface functional groups of Fe_3O_4-WSS NPs with Hg(II) ions enhanced the adsorption processes. But, it was found that beyond 45 min, increasing the contact time had no substantial effect on the adsorption of Hg(II) ions. As contact time was increased beyond 45 min, there was a minor change in the removal rate of Hg(II), resulting from the unavailability of vacant active sites on the adsorbent surface above the equilibrium. Thus, there is strong electrostatic repulsion between Hg(II) ions in the solution and the Hg(II) ions bound to the (OH, C=C, C–O) surface functional groups of Fe_3O_4-WSS NPs. This means at these contact times, the rate of removal of Hg(II) ions becomes slower and slower and the adsorbed Hg(II) ions onto the surface of Fe_3O_4-WSS NPs become in equilibrium with the desorbed Hg(II) from the adsorbent. Awad et al. (2020) and Oveisi et al. (2017) confirmed that the availability of active sites of the surface adsorbents significantly affects the binding of Hg(II) ions with contact time.

Effect of the adsorbent dose on Hg(II) removal

The adsorbent dose on the removal of Hg(II) ion from aqueous solution was investigated at the different amounts of the adsorbent (0.1, 0.4, 0.7, 1, 1.3, and 1.6 g) using 40 mg/L Hg(II) concentration. Then, the solutions were shaken for 75 min at 250 rpm with a pH of 6. Finally, each sample was centrifuged for 5–10 min and filtered by a membrane filter for Hg(II) residual analysis.

As studied, the effect of the adsorbents dose was found to be very critical in the removal of Hg(II) ions (Fig. 7c). The experimental findings demonstrated that as the dose of the Fe_3O_4-WSS NPs increased from 0.1 to 1 g, the percentage removal of Hg(II) ions increased from 74.74 to 98.04%. This shows increased adsorbent dose resulted in increased active sites on the surface of the adsorbent, and therefore, the electrostatic interaction among adsorbent and Hg(II) highly increased, leading to the increase in removal efficiency of Hg(II) ions. However, beyond 1 g of Fe_3O_4-WSS NPs, the percentage removal of Hg(II) ions remains almost constant. This result mainly indicates that the synthesized adsorbent was almost free of aggregation; consequently, the increased adsorbent dosage resulted in similar removal efficiency of the adsorbate as the optimum dosage of Fe_3O_4-WSS NPs. Aggregated adsorbents have a minimum surface area that leads to a decrease in the removal efficiency of the adsorbate (Ahmadijokani et al., 2021). Huang et al. (2016) also indicated the effect of the adsorbent dosages for altered adsorbates and confirmed that increasing the dosage above optimal gets aggregated nanoadsorbent, thereby decreasing the surface area for the binding of the metal ions.

Effect of the initial concentration on Hg(II) removal

The impact of initial Hg(II) concentration on the percentage removal of Hg(II) ions from aqueous solution by Fe_3O_4-WSS NPs was investigated at room temperature by changing the initial concentration (20, 40, 60, 80, and 100 mg/L) and keeping other parameters like adsorbent dose 1 g, contact time 75 min, and pH of 6. The solutions were shaken for 75 min at 250 rpm, and each sample was centrifuged for 5–10 min, filtered by a membrane filter, and the residuals of Hg(II) ions were analyzed.

The effect of initial Hg(II) concentration on the removal of Hg(II) ions is shown in Fig. 7(d). It was shown that an increased initial concentration of Hg(II) ions resulted in a decrease in the percentage removal of Hg(II). The highest and lowest percentage removal was 99.51 and 81.68% at an initial Hg(II) concentration of 20 mg/L and 100 mg/L, respectively. This is because, at a low initial concentration of Hg(II) ions, the probability of the availability of adsorbents' active sites is high and, as a result, can catch up with the available Hg(II) ions. This means the active binding sites of adsorbent Fe_3O_4-WSS NPs are larger than the Hg(II) ions concentration, increasing the attraction between the active binding sites of Fe_3O_4-WSS NPs and the Hg(II) ions. But at high and/or as the initial concentration of Hg(II) increases, some active adsorption sites of the adsorbent become saturated; thus, the removal percentage decreases. This indicates the existence of a small ratio of active binding sites of Fe_3O_4-WSS NPs to the initial Hg(II)

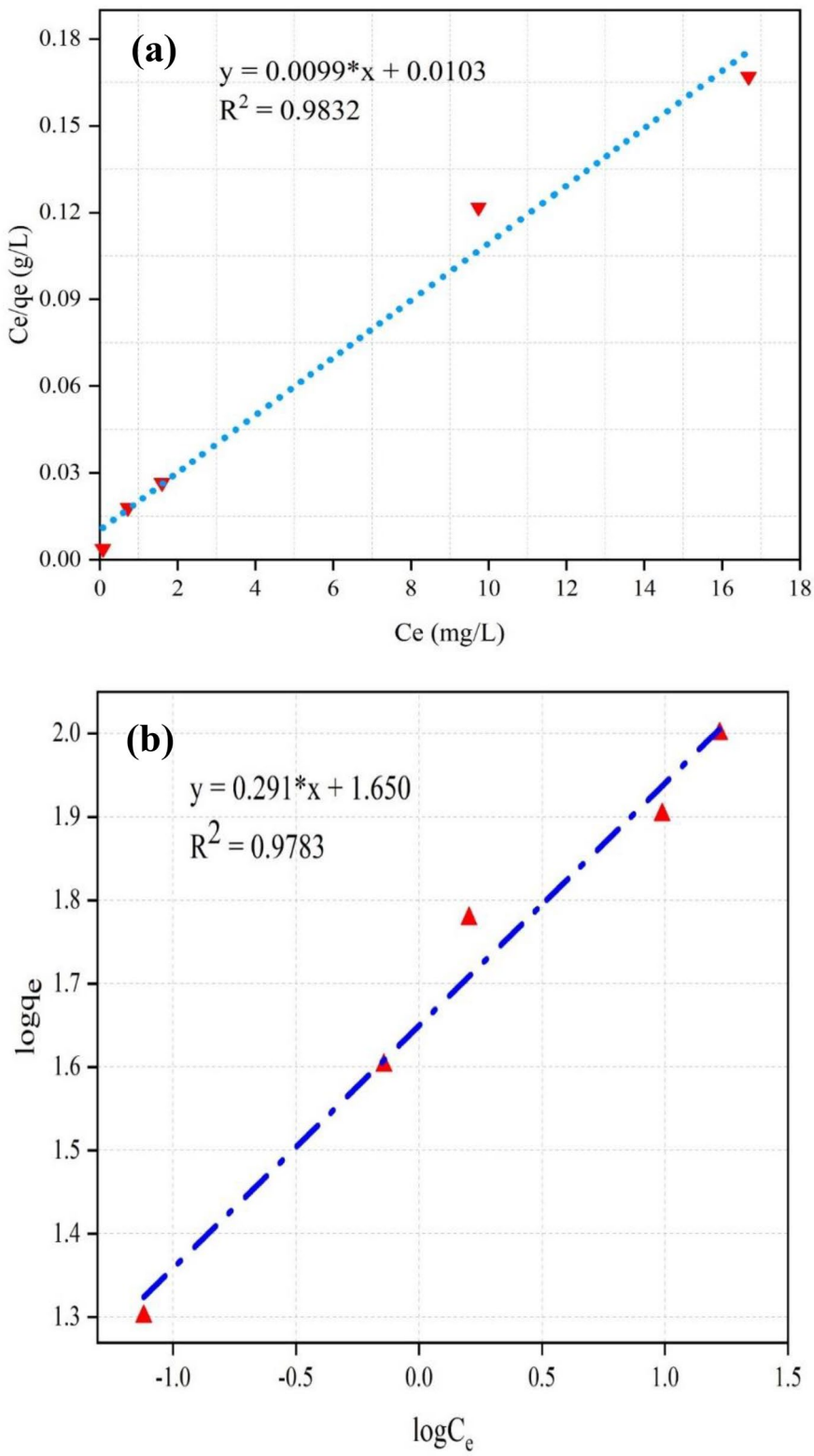

Fig. 8 a Langmuir isotherm model of Hg (II) adsorption; **b** Freundlich isotherm model of Hg (II) adsorption.

Table 3 Langmuir separation factor (RL)

Co	20	40	60	80	100
R_L	0.05	0.03	0.02	0.013	0.01

ions concentration that restricts the removal of Hg(II) ions. Notably, a specified adsorbent dose has a constant number of active adsorption sites that could become saturated above limited initial adsorbate concentrations; thus, nearly the same amount of adsorbate can be adsorbed (Adelaja et al., 2019).

Adsorption isotherm studies

Experimental studies of adsorption isotherms were conducted at optimum conditions. The adsorption behavior among the Fe_3O_4-WSS NPs and Hg(II) ions under different concentrations was elucidated by Langmuir and Freundlich isotherms model (Fig. 8a and b). The results given in Table 4 illustrate the experimental data were fitted with both Langmuir and Freundlich's adsorption isotherm model. But, Fig. 8(a) enlightens that the experimental data results fit better with the Langmuir adsorption isotherm model than the Freundlich isotherm model with a good correlation coefficient (R^2) of 0.983. Thus, it indicates the adsorption of Hg(II) ions on the surface of the Fe_3O_4-WSS NPs effectively undergo the monolayer and homogeneous adsorption process of Hg(II) ions than the multilayer adsorption process. The values of separation factor R_L ($0 < R_L < 1$) given in Table 3 designates the favorability of the adsorption process with a maximum adsorption capacity (q_{max}) of 101.01 mg g^{-1}. Also, a high value of Langmuir coefficient (b) which is 1.00 Lmg^{-1} implies strong binding sites exist on the surface of the adsorbent; thus, the adsorbents can adsorb heavy metals effectively (Bakatula et al., 2014). In another way, the value of Freundlich constant (n), which is greater than 1, indicates a favorable adsorption condition with a correlation coefficient (R^2) of 0.978, representing that a heterogeneous condition can exist. In general, in this study, the Langmuir isotherm model yielded the best fit to the experimental data compared to the Freundlich isotherm model with a high correlation coefficient, as shown in Table 4. These findings of the current study are consistent with the results of Milanović et al. (2021) and Rahbar et al. (2014), which showed the fitness of the data to the Langmuir model with correlation coefficients of 0.996 and 0.949, respectively, thus suggesting that data fitted to the Langmuir model indicates the prepared adsorbent has uniform surface nature. Rahbar et al. (2014) also found the value of separation factor R_L less than one (0.01–0.13), which was similar to the current finding indicating the favorability of the adsorption process on the synthesized nanoparticles. Similarly, the present study revealed the existence of strong binding sites on the surface of Fe_3O_4-WSS NP that enhance the removal of pollutants which was similar to the finding reported on the decolorization of MB and RhB dyes using MoS_2 (Govarthanan et al., 2021).

Conclusions

In the present study, a fresh nano-adsorbent, green-based wheat straw-supported magnetite nanoparticle (Fe_3O_4-WSS NP) was effectively synthesized toward the removal of Hg(II) ions from aqueous solutions. The physicochemical properties of the fabricated Fe_3O_4-WSS NP and the successful binding of wheat straw to the surface of Fe_3O_4 NPs were methodically characterized by FT-IR, SEM, XRD, and TGA. The analysis of XRD and SEM revealed that Fe_3O_4-WSS NPs have average crystalline and particle sizes of 19.83 and 22.48 nm, respectively. Similarly, FT-IR analysis showed the successful adsorption of Hg(II) ions onto the synthesized nano-adsorbent. In the adsorption of Hg(II) onto Fe_3O_4-WSS NPs, it is seen that the pH mainly affects the removal of Hg(II) ions as the adsorption mechanism is highly affected by the electrostatic attraction between the adsorbent and adsorbate. The adsorption isotherm data were fitted

Table 4 Langmuir and Freundlich parameters for the removal of Hg(II) using Fe_3O_4-WSS NPs

Adsorbent	Langmuir isotherm			Freundlich isotherm			
Fe_3O_4-WSS NPs	q_{max} (mg/g)	b (L/mg)	R^2	k_f	n	1/n	R^2
	101.01	1.00	0.983	44.67	3.44	0.29	0.978

very well to the Langmuir isotherm model with a high correlation coefficient and maximum adsorption capacity of 0.983 and 101.01 mg/g, respectively. This study demonstrated that green synthesized wheat straw-supported magnetite NPs are an efficient nano-adsorbent for removing Hg(II) ions.

Acknowledgements The authors sincerely thank the authorities of Jimma Institute of Technology, Jimma University, for providing the financial and laboratory facilities to complete the work successfully. No external funding was involved.

Data availability All data generated or analyzed during this study are included in this article itself.

Code availability Not applicable.

Declarations

Conflict of interest The authors declare no competing interests.

References

Abbas, K., Znad, H., & Awual, M. (2018). A ligand anchored conjugate adsorbent for effective mercury(II) detection and removal from aqueous media. *The Chemical Engineering Journal, 334*, 432–443. https://doi.org/10.1016/j.cej.2017.10.054

Adelaja, O. A., Bankole, A. C., Oladipo, M. E., & Lene, D. B. (2019). Biosorption of Hg(II) ions, Congo red and their binary mixture using raw and chemically activated mango leaves. *International Journal of Energy and Water Resources, 3*(1), 1–12. https://doi.org/10.1007/s42108-019-00012-0

Ahmadijokani, F., Tajahmadi, S., Bahi, A., Molavi, H., Rezakazemi, M., Ko, F., Aminabhavi, T. M., & Arjmand, M. (2021). Ethylenediamine-functionalized Zr-based MOF for efficient removal of heavy metal ions from water. *Chemosphere, 264*, 128466. https://doi.org/10.1016/j.chemosphere.2020.128466

Ahmed, M. A., Ali, S. M., El-Dek, S. I., & Galal, A. (2013). Magnetite-hematite nanoparticles prepared by green methods for heavy metal ions removal from water. *Materials Science and Engineering B: Solid-State Materials for Advanced Technology, 178*(10), 744–751. https://doi.org/10.1016/j.mseb.2013.03.011

Akash, S., Sivaprakash, B., Raja, V. C. V., Rajamohan, N., & Muthusamy, G. (2022). Remediation techniques for uranium removal from polluted environment – Review on methods, mechanism and toxicology. *Environmental Pollution, 302*, 119068. https://doi.org/10.1016/j.envpol.2022.119068

Al-Zoubi, H., Ibrahim, K. A., & Abu-Sbeih, K. A. (2015). Removal of heavy metals from wastewater by economical polymeric collectors using dissolved air flotation process. *Journal of Water Process Engineering, 8*, 19–27. https://doi.org/10.1016/j.jwpe.2015.08.002

Albatrni, H., Qiblawey, H., & El-Naas, M. H. (2021). Comparative study between adsorption and membrane technologies for the removal of mercury. *Separation and Purification Technology, 257*, 117833. https://doi.org/10.1016/j.seppur.2020.117833

Alfredo Reyes Villegas, V., Isaías De León Ramírez, J., Hernandez Guevara, E., Perez Sicairos, S., Angelica Hurtado Ayala, L., & Landeros Sanchez, B. (2020). Synthesis and characterization of magnetite nanoparticles for photocatalysis of nitrobenzene. *Journal of Saudi Chemical Society*, *24*(2), 223–235. https://doi.org/10.1016/j.jscs.2019.12.004

Ali, H., Khan, E., & Ilahi, I. (2019). Environmental chemistry and ecotoxicology of hazardous heavy metals: Environmental persistence, toxicity, and bioaccumulation. *Journal of Chemistry*, *2019*(Cd), 1–14. https://doi.org/10.1155/2019/6730305

AlOmar, M. K., Alsaadi, M. A., Hayyan, M., Akib, S., Ibrahim, M., & Hashim, M. A. (2017). Allyl triphenyl phosphonium bromide based DES-functionalized carbon nanotubes for the removal of mercury from water. *Chemosphere, 167*(2017), 44–52. https://doi.org/10.1016/j.chemosphere.2016.09.133

Altaf, M., Yamin, N., Muhammad, G., Raza, M. A., Shahid, M., & Ashraf, R. S. (2021). Electroanalytical techniques for the remediation of heavy metals from wastewater. In *Water Pollution and Remediation: Heavy Metals* (pp. 471–511). Springer. https://doi.org/10.1007/978-3-030-52421-0_14

Álvarez-Viñas, M., González-Ballesteros, N., Torres, M. D., López-Hortas, L., Vanini, C., Domingo, G., Rodríguez-Argüelles, M. C., & Domínguez, H. (2022). Efficient extraction of carrageenans from Chondrus crispus for the green synthesis of gold nanoparticles and formulation of printable hydrogels. *International Journal of Biological Macromolecules, 206*, 553–566. https://doi.org/10.1016/j.ijbiomac.2022.02.145

Amin, R. M., Mahmoud, R. K., Gadelhak, Y., & Abo El-Ela, F. I. (2021). Gamma irradiated green synthesized zero valent iron nanoparticles as promising antibacterial agents and heavy metal nano-adsorbents. *Environmental Nanotechnology, Monitoring and Management, 16*(2021), 100461. https://doi.org/10.1016/j.enmm.2021.100461

Arun, J., Nirmala, N., Priyadharsini, P., Dawn, S. S., Santhosh, A., Gopinath, K. P., & Govarthanan, M. (2022). A mini-review on bioderived carbon and its nanocomposites for removal of organic pollutants from wastewater. *Materials Letters, 310*, 131476. https://doi.org/10.1016/j.matlet.2021.131476

Awad, F. S., Abouzied, K. M., El-maaty, W. M. A., El-wakil, A. M., & El-shall, M. S. (2020). Effective removal of mercury (II) from aqueous solutions by chemically modified graphene oxide nanosheets. *Arabian Journal of Chemistry, 13*(1), 2659–2670. https://doi.org/10.1016/j.arabjc.2018.06.018

Awual, M. R. (2017). Novel nanocomposite materials for efficient and selective mercury ions capturing from wastewater. *Chemical Engineering Journal, 307*, 456–465. https://doi.org/10.1016/j.cej.2016.08.108

Aziz, A., Agamuthu, P., & Fauziah, S. H. (2018). Removal of bisphenol A and 2,4-Di-tert-butylphenol from landfill

leachate using plant- based coagulant. *Waste Management and Research, 36*(10), 975–984. https://doi.org/10.1177/0734242X18790360

Azizi Haghighat, Z., & Ameri, E. (2016). Synthesis and characterization of nano magnetic wheat straw for lead adsorption. *Desalination and Water Treatment, 57*(21), 9813–9823. https://doi.org/10.1080/19443994.2015.1033475

Bakatula, E. N., Cukrowska, E. M., Weiersbye, I. M., Peter, A., & Tutu, H. (2014). Biosorption of trace elements from aqueous systems in gold mining sites by the filamentous green algae (Oedogonium sp). *Journal of Geochemical Exploration, 144*, 492–503. https://doi.org/10.1016/j.gexplo.2014.02.017

Briffa, J., Sinagra, E., & Blundell, R. (2020). Heavy metal pollution in the environment and their toxicological effects on humans. *Heliyon*, *6*(9), e04691. https://doi.org/10.1016/j.heliyon.2020.e04691

Burange, P. J., Tawar, M. G., Bairagi, R. A., Malviya, V. R., Sahu, V. K., Shewatkar, S. N., Sawarkar, R. A., & Mamurkar, R. R. (2021). Synthesis of silver nanoparticles by using Aloe vera and Thuja orientalis leaves extract and their biological activity: A comprehensive review. *Bulletin of the National Research Centre, 45*(1), 181. https://doi.org/10.1186/s42269-021-00639-2

Buzea, C., & Pacheco, I. (2017). Nanomaterial and nanoparticle: Origin and activity in nanoscience and plant–soil systems. In *Springer, Cham.* (Vol. 48, pp. 71–112). https://doi.org/10.1007/978-3-319-46835-8_3

Camargo, F. P., Sérgio Tonello, P., dos Santos, A. C. A., & Duarte, I. C. S. (2016). Removal of toxic metals from sewage sludge through chemical, physical, and biological treatments—A review. *Water, Air, and Soil Pollution*, *227*(12). https://doi.org/10.1007/s11270-016-3141-3

Cuba-Supanta, G., Guerrero-Sanchez, J., Rojas-Tapia, J., Landauro, C. V., Rojas-Ayala, C., & Takeuchi, N. (2022). An atomistic study on the structural and thermodynamic properties of Al–Fe bimetallic nanoparticles during melting and solidification: The role of size and composition. *Materials Chemistry and Physics, 282*, 125936. https://doi.org/10.1016/j.matchemphys.2022.125936

Dayana Priyadharshini, S., Babu, P. S., Manikandan, S., Subbaiya, R., Govarthanan, M., & Karmegam, N. (2021). Phycoremediation of wastewater for pollutant removal: A green approach to environmental protection and long-term remediation. *Environmental Pollution, 290*, 117989. https://doi.org/10.1016/j.envpol.2021.117989

Ebrahimian Pirbazari, A., Saberikhah, E., & Habibzadeh Kozani, S. S. (2014). Fe3O4-wheat straw: Preparation, characterization and its application for methylene blue adsorption. *Water Resources and Industry, 7–8*(2014), 23–37. https://doi.org/10.1016/j.wri.2014.09.001

El-tawil, R. S., El-wakeel, S. T., Abdel-ghany, A. E., Abuzeid, H. A. M., Selim, K. A., & Hashem, A. M. (2019). Heliyon Silver / quartz nanocomposite as an adsorbent for removal of mercury (II) ions from aqueous solutions. *Heliyon, 5*(2019), e02415. https://doi.org/10.1016/j.heliyon.2019.e02415

Elly, C. T., & Elly, T. (2014). Dithizone procedure for mercury analysis. *Water Pollution Control Federation, 45*(5), 940–945.

Gallego, J. L. R., López-Antón, M. A., de la Rosa, D. M., Rodríguez-Valdés, E., García-González, N., Rodríguez, E., & Martínez-Tarazona, M. R. (2019). Assessment of mercury pollution sources in beach sand and coastal soil by speciation analysis. *Environmental Sciences Europe, 31*(1), 79. https://doi.org/10.1186/s12302-019-0264-3

Gebre, S. H., & Sendeku, M. G. (2019). New frontiers in the biosynthesis of metal oxide nanoparticles and their environmental applications: An overview. *SN Applied Sciences, 1*(8), 1–28. https://doi.org/10.1007/s42452-019-0931-4

Ghosh, S., Bhattacharya, J., Nitnavare, R., & Webster, T. J. (2022). Heavy Metal Removal by *Bacillus* for Sustainable Agriculture. In *Bacilli in Agrobiotechnology* (pp. 1–30). Springer. https://doi.org/10.1007/978-3-030-85465-2_1

Govarthanan, M., Jeon, C. H., & Kim, W. (2022). Synthesis and characterization of lanthanum-based metal organic framework decorated polyaniline for effective adsorption of lead ions from aqueous solutions. *Environmental Pollution, 303*, 119049. https://doi.org/10.1016/j.envpol.2022.119049

Govarthanan, M., Mythili, R., Kim, W., Alfarraj, S., & Alharbi, S. A. (2021). Facile fabrication of (2D/2D) MoS2@MIL-88(Fe) interface-driven catalyst for efficient degradation of organic pollutants under visible light irradiation. *Journal of Hazardous Materials, 414*, 125522. https://doi.org/10.1016/j.jhazmat.2021.125522

Gruskiene, R., Krivorotova, T., Staneviciene, R., Ratautas, D., Serviene, E., & Sereikaite, J. (2018). Preparation and characterization of iron oxide magnetic nanoparticles functionalized by nisin. *Colloids and Surfaces B: Biointerfaces, 169*(2018), 126–134. https://doi.org/10.1016/j.colsurfb.2018.05.017

Guo, Y., Deng, J., Zhu, J., Zhou, X., & Bai, R. (2016). Removal of mercury(II) and methylene blue from a wastewater environment with magnetic graphene oxide: Adsorption kinetics, isotherms and mechanism. *RSC Advances, 6*(86), 82523–82536. https://doi.org/10.1039/c6ra14651a

He, H., Meng, X., Yue, Q., Yin, W., Gao, Y., Fang, P., & Shen, L. (2021). Thiol-ene click chemistry synthesis of a novel magnetic mesoporous silica/chitosan composite for selective Hg(II) capture and high catalytic activity of spent Hg(II) adsorbent. *Chemical Engineering Journal, 405*(1), 126743. https://doi.org/10.1016/j.cej.2020.126743

Hoang, A. T., Nižetić, S., Cheng, C. K., Luque, R., Thomas, S., Banh, T. L., Pham, V. V., & Nguyen, X. P. (2022). Heavy metal removal by biomass-derived carbon nanotubes as a greener environmental remediation: A comprehensive review. *Chemosphere, 287*, 131959. https://doi.org/10.1016/j.chemosphere.2021.131959

Huang, S., Ma, C., Liao, Y., Min, C., Du, P., & Jiang, Y. (2016). Removal of mercury(II) from aqueous Solutions by adsorption on poly(1-amino-5-chloroanthraquinone) nanofibrils: Equilibrium, kinetics, and mechanism studies. *Journal of Nanomaterials, 2016*(6), 1–11. https://doi.org/10.1155/2016/7245829

Husein, D. Z., Hassanien, R., & Khamis, M. (2021). Cadmium oxide nanoparticles/graphene composite: Synthesis, theoretical insights into reactivity and adsorption study. *RSC Advances, 11*(43), 27027–27041. https://doi.org/10.1039/d1ra04754j

Husen, A., & Iqbal, M. (2019). Nanomaterials and plant potential: An overview. In *Nanomaterials and Plant Potential* (pp.3–29). https://doi.org/10.1007/978-3-030-05569-1_1

Jogaiah, S., Paidi, M. K., Venugopal, K., Geetha, N., Mujtaba, M., Udikeri, S. S., & Govarthanan, M. (2021). Phytotoxicological effects of engineered nanoparticles: An emerging nanotoxicology. *Science of the Total Environment, 801*, 149809. https://doi.org/10.1016/j.scitotenv.2021.149809

Kaur, A. (2016). Applications of organo-silica nanocomposites for SPNE of Hg(II). *Applied Nanoscience, 6*(2), 183–190. https://doi.org/10.1007/s13204-015-0413-y

Kavitha, K., Paul, A. J., & J., Kumar, P., Archana, J., Faritha Begam, H., Karmegam, N., & Biruntha, M. (2022). Impact of biosynthesized CuO nanoparticles on seed germination and cyto-physiological responses of Trigonella foenum-graecum and Vigna radiata. *Materials Letters, 313*, 131756. https://doi.org/10.1016/j.matlet.2022.131756

Khan, S., Naushad, M., Govarthanan, M., Iqbal, J., & Alfadul, S. M. (2022). Emerging contaminants of high concern for the environment: Current trends and future research. *Environmental Research, 207*, 112609. https://doi.org/10.1016/j.envres.2021.112609

Khan, F. S. A., Mubarak, N. M., Khalid, M., Walvekar, R., Abdullah, E. C., Mazari, S. A., Nizamuddin, S., & Karri, R. R. (2020). Magnetic nanoadsorbents' potential route for heavy metals removal-a review. *Environmental Science and Pollution Research International, 27*(19), 24342–24356. https://doi.org/10.1007/s11356-020-08711-6

Khandanlou, R., Ahmad, M. B., Shameli, K., & Kalantari, K. (2013). Synthesis and characterization of rice straw/Fe3O4 nanocomposites by a quick precipitation method. *Molecules, 18*(6), 6597–6607. https://doi.org/10.3390/molecules18066597

Kinuthia, G. K., Ngure, V., Beti, D., Lugalia, R., Wangila, A., & Kamau, L. (2020). Levels of heavy metals in wastewater and soil samples from open drainage channels in Nairobi, Kenya: Community health implication. *Scientific Reports, 10*(1), 8434. https://doi.org/10.1038/s41598-020-65359-5

Krishnan, R. Y., Manikandan, S., Subbaiya, R., Biruntha, M., Govarthanan, M., & Karmegam, N. (2021). Removal of emerging micropollutants originating from pharmaceuticals and personal care products (PPCPs) in water and wastewater by advanced oxidation processes: A review. *Environmental Technology and Innovation, 23*, 101757. https://doi.org/10.1016/j.eti.2021.101757

Krishnani, K. K., Choudhary, K., Boddu, V. M., Moon, D. H., & Meng, X. (2021). Heavy metals biosorption mechanism of partially delignified products derived from mango (Mangifera indica) and guava (Psidium guiag) barks. *Environmental Science and Pollution Research, 28*(25), 32891–32904. https://doi.org/10.1007/s11356-021-12874-1

Kumar, R., Rauwel, P., & Rauwel, E. (2021). Nanoadsorbants for the removal of heavy metals from contaminated water: Current scenario and future directions. In *Processes* (Vol. 9, Issue 8, p. 1379). https://doi.org/10.3390/pr9081379

Lazzarini, A., Colaiezzi, R., Passacantando, M., D'Orazio, F., Arrizza, L., Ferella, F., & Crucianelli, M. (2021). Investigation of physico-chemical and catalytic properties of the coating layer of silica-coated iron oxide magnetic nanoparticles. *Journal of Physics and Chemistry of Solids, 153*, 110003. https://doi.org/10.1016/j.jpcs.2021.110003

López, Y. C., & Antuch, M. (2020). Morphology control in the plant-mediated synthesis of magnetite nanoparticles. *Current Opinion in Green and Sustainable Chemistry, 24*, 32–37. https://doi.org/10.1016/j.cogsc.2020.02.001

Mahbubul, I. M. (2019). Introduction to Nanofluid. In I. M. B. T.-P. Mahbubul Characterization, Properties and Application of Nanofluid (Ed.), *Preparation, Characterization, Properties and Application of Nanofluid,* 1–13. William Andrew Publishing. https://doi.org/10.1016/b978-0-12-813245-6.00001-0

Malavika, J. P., Shobana, C., Ragupathi, M., Kumar, P., Lee, Y. S., Govarthanan, M., & Selvan, R. K. (2021). A sustainable green synthesis of functionalized biocompatible carbon quantum dots from Aloe barbadensis Miller and its multifunctional applications. *Environmental Research, 200*, 111414. https://doi.org/10.1016/j.envres.2021.111414

Marimón-bolívar, W., & González, E. E. (2018). Study of agglomeration and magnetic sedimentation of Glutathione @ Fe 3 O 4 nanoparticles in water medium • Estudio de aglomeración y sedimentación magnética de nanopartículas de Glutatión @ Fe 3 O 4 en medio acuoso. *Dyna rev.fac.nac.minas*, *85*(205), 19–26. https://doi.org/10.15446/dyna.v85n205.68245

Milanović, M., Stijepović, I., Obrenović, Z., Kukić, D., Vasić, V., Panić, S., & Šćiban, M. (2021). Chromium(VI) adsorption onto boehmite nanoparticles obtained by cost effective "green" synthesis. *International Journal of Environmental Science and Technology, 18*(11), 1–12. https://doi.org/10.1007/s13762-021-03819-9

Muldarisnur, M., Fridayanti, N., Oktorina, E., Zeni, E., Elvaswer, E., & Syukri, S. (2019). Effect of nanoparticle geometry on sensitivity of metal nanoparticle based sensor. *IOP Conference Series: Materials Science and Engineering, 578*(1), 012036. https://doi.org/10.1088/1757-899X/578/1/012036

Muthiah, M., Park, I. K., & Cho, C. S. (2013). Surface modification of iron oxide nanoparticles by biocompatible polymers for tissue imaging and targeting. *Biotechnology Advances, 31*(8), 1224–1236. https://doi.org/10.1016/j.biotechadv.2013.03.005

Nande, A., Raut, S., Michalska-Domanska, M., & Dhoble, S. J. (2020). Green Synthesis of Nanomaterials Using Plant Extract: A review. *Current Pharmaceutical Biotechnology, 22*(13), 1794–1811. https://doi.org/10.2174/1389201021666201117121452

Naseem, T., & Durrani, T. (2021). The role of some important metal oxide nanoparticles for wastewater and antibacterial applications: A review. *Environmental Chemistry and Ecotoxicology, 3*(2021), 59–75. https://doi.org/10.1016/j.enceco.2020.12.001

Nikolova, M. P., & Chavali, M. S. (2020). Metal oxide nanoparticles as biomedical materials. *Biomimetics, 5*(2), 1–47. https://doi.org/10.3390/BIOMIMETICS5020027

Nurfatini, B., & Amir, S. (2018). Recent advances in mercury detection; towards enabling a sensitive and rapid point-of-check measurement. *Journal of Toxicology and Risk Assessment*, *4*(1), 1–10. https://doi.org/10.23937/2572-4061.1510010

Oveisi, F., Nikazar, M., Razzaghi, M. H., Mirrahimi, M. A. S., & Jafarzadeh, M. T. (2017). Effective removal of mercury from aqueous solution using thiol-functionalized magnetic nanoparticles. *Environmental Nanotechnology, Monitoring and Management, 7*(1), 130–138. https://doi.org/10.1016/j.enmm.2017.01.004

Pakzad, K., Alinezhad, H., & Nasrollahzadeh, M. (2019). Green synthesis of Ni@Fe3O4 and CuO nanoparticles using Euphorbia maculata extract as photocatalysts for the degradation of organic pollutants under UV-irradiation. *Ceramics International, 45*(14), 17173–17182. https://doi.org/10.1016/j.ceramint.2019.05.272

Pandey, L. M. (2021). Surface engineering of nano-sorbents for the removal of heavy metals: Interfacial aspects. *Journal of Environmental Chemical Engineering*, *9*(1), 104586. https://doi.org/10.1016/j.jece.2020.104586

Prakash, M., Kavitha, H. P., Abinaya, S., Vennila, J. P., & Lohita, D. (2022). Green synthesis of bismuth based nanoparticles and its applications - A review. *Sustainable Chemistry and Pharmacy, 25*, 100547. https://doi.org/10.1016/j.scp.2021.100547

Qiao, R., Yang, C., & Gao, M. (2009). Superparamagnetic iron oxide nanoparticles: From preparations to in vivo MRI applications. *Journal of Materials Chemistry, 19*(35), 6274–6293. https://doi.org/10.1039/b902394a

Rahbar, N., Jahangiri, A., Boumi, S., & Khodayar, M. J. (2014). Mercury removal from aqueous solutions with chitosan-coated magnetite nanoparticles optimized using the box-behnken design. *Jundishapur Journal of Natural Pharmaceutical Products*, *9*(2), e15913. https://doi.org/10.17795/jjnpp-15913

Rahman, M. M., Hossain, M. K. F. B., Afrin, S., Saito, T., & Kurasaki, M. (2022). *Effects of Metals on Human Health and Ecosystem,* 1–39. Springer. https://doi.org/10.1007/698_2021_825

Rajasulochana, P., & Preethy, V. (2016). Comparison on efficiency of various techniques in treatment of waste and sewage water – A comprehensive review. *Resource-Efficient Technologies, 2*(4), 175–184. https://doi.org/10.1080/01496395.2014.968261

Rauwel, P., Küünal, S., Ferdov, S., & Rauwel, E. (2015). A review on the green synthesis of silver nanoparticles and their morphologies studied via TEM. *Advances in Materials Science and Engineering, 2015*(2015), 1–8. https://doi.org/10.1155/2015/682749

Roohi, S., Dubey, S., Sheoran, H. S., Kumar, V., & Kaushik, G. (2021). Potential of green nanoparticles for sensing and remediation of heavy metals from mining applications. In *Green Nanomaterials for Industrial Applications,* 445–476. Elsevier. https://doi.org/10.1016/B978-0-12-823296-5.00017-4

Saleh, T. A., Mustaqeem, M., & Khaled, M. (2021). Developing water treatment technologies in removing heavy metals from wastewater: A review. *Environmental Nanotechnology, Monitoring & Management, 17*, 100617. https://doi.org/10.1016/j.enmm.2021.100617

Salehipour, M., Rezaei, S., Mosafer, J., Pakdin-Parizi, Z., Motaharian, A., & Mogharabi-Manzari, M. (2021). Recent advances in polymer-coated iron oxide nanoparticles as magnetic resonance imaging contrast agents. *Journal of Nanoparticle Research, 23*(2), 48. https://doi.org/10.1007/s11051-021-05156-x

Samal, K., Bandyopadhyay, R., & Dash, R. R. (2022). Biological Treatment of Contaminants of Emerging Concern in Wastewater: A Review. *Journal of Hazardous, Toxic, and Radioactive Waste, 26*(2), 4022002. https://doi.org/10.1061/(asce)hz.2153-5515.0000685

Sandhya, J., & Kalaiselvam, S. (2020). Biogenic synthesis of magnetic iron oxide nanoparticles using inedible borassus flabellifer seed coat: Characterization, antimicrobial, antioxidant activity and in vitro cytotoxicity analysis. *Materials Research Express, 7*(1), 15045. https://doi.org/10.1088/2053-1591/ab6642

Scopel, E., Conti, P. P., Stroppa, D. G., & Dalmaschio, C. J. (2019). Synthesis of functionalized magnetite nanoparticles using only oleic acid and iron (III) acetylacetonate. *SN Applied Sciences, 1*(2), 1–8. https://doi.org/10.1007/s42452-018-0140-6

Silva, V. A. J., Andrade, P. L., Silva, M. P. C., Bustamante, A. D., Valladares, D. L. S., & L., & Albino Aguiar, J. (2013). Synthesis and characterization of Fe3O4 nanoparticles coated with fucan polysaccharides. *Journal of Magnetism and Magnetic Materials, 343*(2013), 138–143. https://doi.org/10.1016/j.jmmm.2013.04.062

Singh, J., Dutta, T., Kim, K.-H., Rawat, M., Samddar, P., & Kumar, P. (2018). 'Green' synthesis of metals and their oxide nanoparticles: Applications for environmental remediation. *Journal of Nanobiotechnology, 16*(1), 84. https://doi.org/10.1186/s12951-018-0408-4

Singh, S., Chaudhary, I. J., & Kumar, P. (2019). Utilization of low-cost agricultural waste for removal of toxic metals from environment : A review. *International Journal of Scientific Research in Biological Sciences*, *6*(4), 56–61. https://doi.org/10.26438/ijsrbs/v6i4.5661

Sivaranjanee, R., Senthil Kumar, P., Saravanan, R., & Govarthanan, M. (2022). Electrochemical sensing system for the analysis of emerging contaminants in aquatic environment: A review. *Chemosphere, 294*, 133779. https://doi.org/10.1016/j.chemosphere.2022.133779

Sivasubramaniyan, S. G., Kandasamy, S., Manickam, N., & kumar. (2022). Novel biotechnological approaches for removal of emerging contaminants. *Biotechnology for Zero Waste*. https://doi.org/10.1002/9783527832064.ch26

Somu, P., Kannan, U., & Paul, S. (2019). Biomolecule functionalized magnetite nanoparticles efficiently adsorb and remove heavy metals from contaminated water. *Journal of Chemical Technology and Biotechnology, 94*(6), 2009–2022. https://doi.org/10.1002/jctb.5984

Taux, K., Kraus, T., & Kaifie, A. (2022). Mercury exposure and its health effects in workers in the Artisanal and Small-Scale Gold Mining (ASGM) sector—A systematic review. *International Journal of Environmental Research and Public Health, 19*(4), 2081. https://doi.org/10.3390/ijerph19042081

Vega-Páez, J. D., Rivas, R. E., & Dussán-Garzón, J. (2019). High efficiency mercury sorption by dead biomass of Lysinibacillus sphaericus-New insights into the treatment of contaminated water. *Materials, 12*(8), 1–13. https://doi.org/10.3390/ma12081296

Vélez, E., Campillo, G. E., Morales, G., Hincapié, C., Osorio, J., Arnache, O., Uribe, J. I., & Jaramillo, F. (2016). Mercury removal in wastewater by iron oxide nanoparticles. *Journal of Physics: Conference Series, 687*(1), 1–4. https://doi.org/10.1088/1742-6596/687/1/012050

Venkateswarlu, S., & Yoon, M. (2015). Surfactant-free green synthesis of Fe3O4 nanoparticles capped with 3,4-dihydroxyphenethylcarbamodithioate: Stable recyclable magnetic nanoparticles for the rapid and efficient removal

of Hg(II) ions from water. *Dalton Transactions, 44*(42), 18427–18437. https://doi.org/10.1039/c5dt03155a

Vs, T., Klc, I., Cs, E., & Otitoju, O. (2017). *Biosorption kinetics of heavy metals from fertilizer industrial waste water using groundnut husk powder as an adsorbent*. *2*(6), 221–228. https://doi.org/10.15406/jabb.2017.02.00049

Wen, Y. H., Li, L., Li, Y. M., Zhao, T., & Huang, R. (2021). Molecular dynamics simulations of thermally induced surface and shape evolution of concave Au nanocubes: Implications for Catalysis. *ACS Applied Nano Materials, 4*(9), 9527–9535. https://doi.org/10.1021/acsanm.1c01994

Xiang, L., Niu, C. G., Tang, N., Lv, X. X., Guo, H., Li, Z. W., Liu, H. Y., Lin, L. S., Yang, Y. Y., & Liang, C. (2021). Polypyrrole coated molybdenum disulfide composites as adsorbent for enhanced removal of Cr(VI) in aqueous solutions by adsorption combined with reduction. *Chemical Engineering Journal, 408*, 127281. https://doi.org/10.1016/j.cej.2020.127281

Xu, W., Yang, T., Liu, S., Du, L., Chen, Q., Li, X., Dong, J., Zhang, Z., Lu, S., Gong, Y., Zhou, L., Liu, Y., & Tan, X. (2022). Insights into the Synthesis, types and application of iron Nanoparticles: The overlooked significance of environmental effects. *Environment International, 158*, 106980. https://doi.org/10.1016/j.envint.2021.106980

Yang, C. (2012). A green and facile approach for synthesis of magnetite nanoparticles with tunable sizes and morphologies. *Materials Letters, 73*(2), 129–132. https://doi.org/10.1016/j.matlet.2012.01.031

Yang, J., Hou, B., Wang, J., Tian, B., Bi, J., Wang, N., Li, X., & Huang, X. (2019a). Nanomaterials for the removal of heavy metals from wastewater. *Nanomaterials*, *9*(3). https://doi.org/10.3390/nano9030424

Yang, J., Hou, B., Wang, J., Tian, B., Bi, J., Wang, N., Li, X., & Huang, X. (2019b). Nanomaterials for the removal of heavy metals from wastewater. *Nanomaterials, 9*(3), 424. https://doi.org/10.3390/nano9030424

Yazdani, F., Fattahi, B., & Azizi, N. (2016). Synthesis of functionalized magnetite nanoparticles to use as liver targeting MRI contrast agent. *Journal of Magnetism and Magnetic Materials, 406*(2016), 207–211. https://doi.org/10.1016/j.jmmm.2016.01.026

Zhao, J., Luan, L., Li, Z., Duan, Z., Li, Y., Zheng, S., Xue, Z., Xu, W., & Niu, Y. (2020). The adsorption property and mechanism for Hg(II) and Ag(I) by Schiff base functionalized magnetic Fe3O4 from aqueous solution. *Journal of Alloys and Compounds, 825*(2020), 154051. https://doi.org/10.1016/j.jallcom.2020.154051